Accepted Manuscript

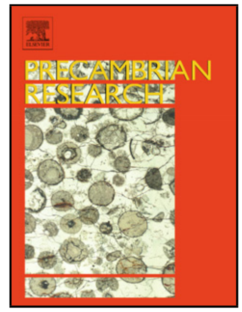


Title: Delineating and characterizing the boundary of the Cathaysia Block and the Jiangnan orogenic belt in South China

Author: Jinlong Yao Liangshu Shu Peter A. Cawood Jinyi Li

PII: S0301-9268(16)00032-2
DOI: http://dx.doi.org/doi:10.1016/j.precamres.2016.01.023
Reference: PRECAM 4442

To appear in: *Precambrian Research*

Received date: 4-8-2015
Revised date: 7-1-2016
Accepted date: 11-1-2016

## Research highlights

- Ca. 880~850 Ma rock units identified within the Jiangshan-Shaoxing fault zone at Shijiao indicate a convergent plate margin setting
- Field geology and analytical data indicate the Shijiao area display close affinity with Jiangnan belt rather than Cathaysia
- Overall relationships at Shijiao constrain the location of suture between Cathaysia and Jiangnan in NE Zhejiang during Neoproterozoic.

# Delineating and characterizing the boundary of the Cathaysia Block and the Jiangnan orogenic belt in South China

Jinlong Yao[a], Liangshu Shu[a,*], Peter A. Cawood[b, c], Jinyi Li[d]

[a] State Key Laboratory for Mineral Deposits Research, School of Earth Sciences and Engineering, Nanjing University, Nanjing 210093, China

[b] Department of Earth Sciences, University of St Andrews, North Street, St Andrews KY16 9AL, UK

[c] School of Earth and Environment, The University of Western Australia, 35 Stirling Highway, Crawley, WA 6009, Australia

[d] Institute of Geology, Chinese Academy of Geological Sciences, Beijing 100037, China

* Corresponding author E–mail: Lsshu@nju.edu.cn

## Abstract

The Jiangshan-Shaoxing fault zone lies along the SE margin of the Jiangnan belt, and delineates the northeastern margin of the Cathaysia Block of the South China Craton. At Shijiao in NE Zhejiang, the fault zone consists of hornblende schist intruded by migmatized quartz diorite. It constitutes a shear zone delineating the welded boundary between the Neoproterozoic Shuangxiwu Group of Jiangnan belt to the north and the Chencai Complex of Cathaysia Block to the south. The Shuangxiwu Group is composed mainly of basalt, andesite and flysch, whereas the Chencai

Complex contains magmatic and sedimentary rocks that experienced amphibolite facies metamorphism. Zircons from quartz diorite and gabbro from the fault zone at Shijiao yield ages of 854 ± 6 Ma, 857 ± 5 Ma and 860 ± 5 Ma, with positive εHf(t) values of 7.81~11.8 and 4.57~10.39. The quartz diorite and mafic-ultramafic rock samples display minor LREE enriched pattern with obvious depletion of Nb, Ta, Rb, Ba and Ti, compared to their neighboring elements and plot in the volcanic arc field on geochemical diagrams, similar to that of volcanic rocks from Shuangxiwu Group. Overall relationships within the Jiangshan-Shaoxing fault zone at Shijiao suggest the ca. 860-850 Ma rock suites were generated in a convergent plate margin and are part of the Jiangnan belt, and not the Cathaysia Block, thus constraining the location of the suture between the two lithotectonic units in NE Zhejiang area during Neoproterozoic.

**Keywords: Jiangshan-Shaoxing fault zone; quartz diorite; Geochronology; Neoproterozoic arc suites; tectonic affinity; South China**

## 1. Introduction

The Neoproterozoic Jiangshan-Shaoxing fault zone delineates the SE margin of the Jiangnan orogenic belt, which is an assemblage of Neoproterozoic convergent plate margin accretionary successions that record the assembly of the Cathaysia and Yangtze blocks in South China Craton (Fig. 1; Cawood et al., 2013). The age and nature of the arc-trench successions as well as their number and direction of subduction, along with the overall crustal evolution of the orogenic belt and timing of final assembly between Yangtze and Cathaysia blocks, are disputed (Shu, 2012;

Wang et al., 2014; Yao et al., 2014a, b, 2015; Zhao, 2015). This uncertainty in the evolution of the orogen has resulted in controversy as to whether South China occupies an internal or marginal position in the Rodinia supercontinent (Cawood et al., 2013; Wang et al., 2013b).

The northeast-southwest trending Jiangshan-Shaoxing fault zone can be traced for up to 800 km and is up to 30 km wide (Shu, 2012). The fault is considered to constitute the southeastern boundary of the Jiangnan orogen with the Cathaysia Block. In the vicinity of Shijiao (Zhejiang Province), within the fault zone, constituent rock suites are similar to those of the Jiangnan belt, but metamorphic grade is higher and similar to that in the adjoining Chencai metamorphic complex to the southeast, which forms part of the Cathaysia Block (Fig. 2, BGMRZJ, 1989; Zhao and Sun, 1994), or alternatively has been interpreted to form the NE extent of the Jiangshan-Shaoxing fault zone as a Neoproterozoic suture (Shu et al., 2006). These relations have led to suggestions that the rocks within the fault zone may constitute part of supra-subduction zone units on the margin of the Cathaysia Block (e.g., Zhao, 2015). This in turn has implications for the Neoproterozoic crustal evolution of South China and, in particular, whether southeast-directed subduction took place beneath the margin of the Cathaysia Block (e.g., Wang et al., 2014; Zhao, 2015). Our study outlines field, geochemical and isotopic data on migmatized quartz diorite and mafic-ultramafic rocks in the fault zone, along with volcanic rocks and associated sedimentary rocks of the adjoining Shuangxiwu Group from the Jiangnan belt to the northwest (Fig. 2). Our results indicate that fault zone lithologies are an accretionary assemblage within the Jiangnan belt rather than the Cathaysia Block, thus delinating the boundary between the two lithotectonic assemblages at Shijiao. Furthermore, they demonstrate the presence of ca. 880 to 850 Ma convergent plate margin units in the eastern Jiangnan belt, providing an additional constraint on the age of final assembly between Yantze and Cathaysia blocks.

## 2. Geological setting and litho-stratigraphic structures

### *2.1. Geological setting*

The South China Craton consists of the Yangtze Block to the northwest and Cathaysia Block to the southeast, sutured along the Jiangnan orogenic belt. The former is composed of an Archean–Paleoproterozoic crystalline basement surrounded by Neoproterozoic orogenic belts (Panxi-Hannan belt and Jiangnan belt) that underwent mid-Neoproterozoic greenschist facies metamorphism (Fig. 1; Shu, 2012; Zhao and Cawood, 2012). These units are overlain by middle-late Neoproterozoic to Phanerozoic strata (Charvet et al., 2010; Wang et al., 2013a, 2014; Dong et al., 2015). The Cathaysia Block contains numerous Neoproterozoic-Paleozoic meta-sedimentary and meta-igneous rocks, as well as minor Paleoproterozoic meta-igneous rocks (Zhao and Cawood, 2012; Shu, 2012; Shu et al., 2014, 2015). Paleozoic regional metamorphism of amphibolite facies along with coeval deformation, crustal partial melting and granite emplacement, are distinctive features of the Cathaysia Block compared to the Jiangnan belt (Shu, 2006; Li et al., 2010).

### 2.1. Lithology and related structures

The greenschist facies early Neoproterozoic Shuangxiwu Group (Pt3sh) is the oldest unit exposed in the eastern Jiangnan belt in northern Zhejiang Province, and is unconformably overlain by a northwest dipping middle Neoproterozoic succession, the Heshangzheng Group (Pt3h), and the latest Neoproterozoic Sinian System (Pt3z) that are essentially unmetamorphosed (Fig. 2, 3a, 3b; BGMRZJ, 1989). The Shuangxiwu Group is divided into the Pingshui, Beiwu, Yanshan and Zhangcun formations. The Pingshui and Yanshan formations consist predominantly of intermediate-acidic volcanic rocks, whereas the Beiwu Formation is composed mainly of intermediate-basic volcanic rocks. The Zhangcun Formation contains a series of continental derived sedimentary rocks (tuff and tuffaceous sandstones and siltstones) (BGMRZJ, 1989). The volcanic rocks from the Pingshui Formation are dated at 978 ± 44 Ma (Sm–Nd whole rock isochron, Zhang et al., 1990) and 904 ± 8 Ma and 906 ± 10 Ma (LA-ICPMS U–Pb zircon, Chen et al., 2009). Andesitic rocks from the Beiwu and Zhangcun formations yield discordant U-Pb $^{206}Pb/^{238}U$ zircon ages of 926 ± 15 Ma and 891 ± 12 Ma (Li et al., 2009). The unconformably overlying middle Neoproterozoic Heshangzheng Group has a maximum depositional age of ca. 820 Ma as constrained by detrital zircons (Yao et al., 2013). It consists of an interstratified succession of conglomerate, sandstone, siltstone and mudstone, with interbedded tuff and muddy limestone Fig. 3).

In the Shijiao area, within the Jiangshan-Shaoxing fault zone, exposed rock units are mainly migmatized hornblende schist intruded by migmatized quartz diorite, along with minor meta-rhyolite (Fig. 2). Amphibole pyroxenite along with minor gabbro and dunite occur as blocks within the quartz diorite (Fig. 4). Minor nodular ultramafic rocks occur in the transition zone between ultramafic rocks and migmatized quartz diorite (Zhou et al., 1993). Rock units within the fault zone are metamorphosed to amphibolite facies. Zircon ages of 879 ± 10 Ma (LA-ICPMS U–Pb; Yao et al., 2014a) and 838 ± 5 Ma (SHRIMP U-Pb; Li et al. (2010) have been obtained from the hornblende schist and meta-rhyolite, respectively. Local mylonitization also occurs in the diorite and has been dated at 370 ± 10 Ma (K–Ar on biotite), 353 Ma and 361 Ma (Ar–Ar on biotite, with unknown errors and data quality cannot be evaluated) (Zhu and Zhou, 1994).

The Chencai metamorphic complex, which lies to the southeast of the Jiangshan-Shaoxing fault zone (Fig. 1, Fig. 2; BGMRZJ, 1989), consists of plagioclase gneiss, amphibolite, and leucocratic gneiss interbanded with schist, leptynite, marble and minor quartzite (BGMRZJ, 1989). Protoliths of the complex are considered to be Neoproterozoic in age that experienced Paleozoic amphibolite facies metamorphism and coeval deformation (Yao et al., 2014a; Shu et al., 2015). The unit also shows widespread migmatization. Zircon SHRIMP U–Pb ages of 857 ± 7 and 841 ± 12 are reported from meta-gabbro within the complex (Li et al., 2010; Shu et al. 2011). An intercept age of 1781 ± 21 Ma inferred from SHRIMP zircon U–Pb ages has also been obtained from amphibolite and interpreted as the formation age of gabbroic protolith (Li et al., 2010). Metamorphism is dated at 426 ± 2 Ma based on $^{40}Ar/^{39}Ar$ age on hornblende and 426 ± 7 Ma by $^{40}Ar/^{39}Ar$ age on biotite (Li et al., 2010). Zircon U–Pb ages of 453 ± 4 Ma and 438 ± 4 Ma are reported from the migmatite and gabbro inclusions within the Chencai Complex (Yao et al. 2014a).

### *2.2. Sample descriptions*

Sample locations are shown on figures 2 and 3 and include 2 quartz diorites (1194 and 1194-1; GPS: N25°45.919', E109°50.071') and 12 mafic-ultramafic rocks (1472, 1472-4, 1472-6, 1472-7, 1472-8, 1472-11, 1472-12, 1472-13, 1472-14, 1472-15, 1472-17 and 1472-18; GPS: N29°33.220', E120°10.296') from within the Jiangshan-Shaoxing fault zone (Fig. 2). Two andesitic porphyrite samples (1468-1, 1468-4; GPS: N29°54.064', E119°58.437'), one pyroclastic sample (1470; GPS: N29°52.533', E120°01.268') and one basalt sample (1467-2; GPS: N29°52.533', E120°01.268') were also collected from the Shuangxiwu Group (Fig. 2, Fig. 4).

The quartz diorite samples 1194, 1194-1 contain about 65% plagioclase, 20% hornblende and 15% quartz. Gabbro sample 1472 contains some 60% plagioclase, 25% clinopyroxene, 10% hornblende, 5% opaque mineral oxide and other accessory mineral such as titanite, whereas gabbro sample 1172-4 has 35% plagioclase, 45% clinopyroxene and 5% olivine, along with 10% hornblende and 5% accessory minerals (opaque oxide). Other gabbro samples 1472-07, 1472-12, 1472-13, 1472-15, and 1472-18 are mainly composed of 15~25% plagioclase, 50~65% clinopyroxene and 10% hornblende. Amphibole pyroxenite samples 1472-6, 1472-8, 1472-11, 1472-14 and 1472-17 contain about 60% clinopyroxene, 30% hornblende and 10% magnetite and other accessory minerals. Two andesitic porphyrite samples (1468-1, 1468-4) mainly contain phenocrysts of plagioclase, which occur in a fine grained to glassy matrix. The pyroclastic rock sample (1470) is foliated and composed of muscovite, quartz, plagioclase and rock fragments (Fig. 5).

The diorite samples (1194 and 1494-1) and gabbro sample 1472 were selected for zircon U–Pb dating and Hf isotope analysis. These along with the remaining samples were analyzed for whole rock geochemistry.

## 3. Analytical procedures

Zircons were separated from the crushed rocks using heavy liquid and magnetic techniques and then handpicked under a binocular microscope. The zircon grains were mounted in epoxy resin, polished and coated. Cathodoluminescence (CL) images of the zircons were obtained using a Quanta 400 FEG electron microscope equipped with Mono CL3+ (Gatan, U.S.A.) at the State Key Laboratory of Continental Dynamics in Northwest University.

The zircon U–Pb isotopic dating was carried out at the State Key Laboratory for Mineral Deposits Research in Nanjing University, using an Agilent 7500a ICP–MS connected to a New Wave 213 nm laser ablation system. U–Pb fractionation was corrected using zircon standard GEMOC GJ–1 with an age of 601 ± 12 Ma and accuracy was controlled by using the zircon standard Mud Tank with an age of 735 ± 12 Ma. The U–Pb ages were calculated from the original signal data using the Glitter software and U–Th–Pb age data are plotted on concordia diagrams using the Isoplot program (Ludwig, 2003). Zircons older than 1000 Ma have high contents of radiogenic Pb, hence $^{207}Pb/^{206}Pb$ age is more reliable and used to determine the crystallization age. On the other hand, due to low content of radiogenic Pb, the $^{206}Pb/^{238}U$ age is more reliable for zircons with ages younger than 1000 Ma.

The zircon Hf isotopes were analyzed using a Neptune MC–ICP–MS at the State Key Laboratory for Mineral Deposits Research in Nanjing University. Zircon standard 91500 was used for external correction and has a $^{176}Hf/^{177}Hf$ value of 0.282300 ± 8 (2σ). Initial $^{176}Hf/^{177}Hf$ values were calculated based on Lu decay constant of 1.865E–11 (Scherer et al., 2001). The Hf model ages were calculated under the assumption that the $^{176}Lu/^{177}Hf$ of average crust is 0.015, and the $^{176}Hf/^{177}Hf$ and $^{176}Lu/^{177}Hf$ ratios of chondrite and depleted mantle at the present time are 0.282772 and 0.0332, 0.28325 and 0.0384 (Blichert-Toft and Albarede, 1997).

Whole rock major element analyses were performed using an ARL9800XP+ X–ray fluorescence spectrometer (XRF) at the State Key Laboratory for Mineral Deposits Research in Nanjing University. The analytical precision is generally better than 2% for all elements. Trace element abundances were measured using a Finnigan Element II ICP–MS at the State Key Laboratory of Mineral Deposit Research, Nanjing University, which gives precision better than 10% for most of the analyzed elements.

## 4. Analytical results

### *4.1. Zircon U–Pb dating and Hf isotopes*

Zircons obtained from gabbro (1472) and diorite (1194, 1194-1) samples are mostly euhedral prismatic grains. Most of the grains show banded or sector zoning in CL images (Fig. 6). A total of 32 grains from gabbro sample 1472 were analyzed, yielding a main age range of 953–847 Ma and giving a weighted average $^{206}Pb/^{238}U$

age of 860 ± 5 Ma (MSWD = 0.08, n = 24) (Fig. 6). Among twenty-two analyses from quartz diorite sample 1194, 18 U–Pb dating analyses yield a weighted average $^{206}Pb/^{238}U$ age of 854 ± 6 Ma (MSWD = 0.2, n = 18) (Fig. 6). Twenty analyses were conducted on zircons from gabbro sample 1472, yielding an age range of 871–857 Ma and a weighted average $^{206}Pb/^{238}U$ age of 857 ± 5 Ma (MSWD = 0.24, n = 20). These weighted mean ages are interpreted as the crystallization age of the gabbro and diorite samples. The Th/U ratios of the zircons from gabbro and diorite sample range from 0.66 to 3.39 and 0.75 to 1.57, respectively (Table 1).

Zircons from quartz diorite samples 1194 and 1194-1 display present day $^{176}Hf/^{177}Hf$ ratios of 0.282378–0.282558 and yield positive εHf(t) values of 7.81~11.8 and 4.57~10.42, respectively (Table 2). This equates to Hf model ages of 1.0~1.2 Ga (Figure. 7), suggesting the presence of latest Mesoproterozoic juvenile mantle material in this region.

### *4.2. Major and trace element compositions*

Major and trace element analytical results are presented in Table 3. Our discussion focuses mainly on the immobile elements and element ratios due to low-grade alteration of the rock units and the possibility of mobilization of elements with a large ionic radius to charge during low-grade metamorphism (Pearce and Cann, 1973; Wood, 1980; Wyman, 1999). On the $Zr/TiO_2$–Nb/Y diagram, the studied samples fall in the basalt and andesite field (Fig. 8).

The quartz diorite samples (1194 and 1194-1) have low $TiO_2$ (0.62 %), $SiO_2$ (55.56–55.83 %) and $Na_2O$ (4.61–4.63 %), with high Mg# of 49 (Table 3). The coarse grained gabbros (1472) also display low values of $TiO_2$ (1.02 %), $SiO_2$ (44.9 %) and $Na_2O$ (0.72 %), with Mg# of 49. Other mafic and ultramafic rock samples from the Shijiao area within the Jiangshan-Shaoxing fault zone display a wide range of compositions of $SiO_2$ (33.33 to 53.46 %), MgO (9.93–23.4 %) and $FeO^t$ (12.09–26.52%), and low $Al_2O_3$ (3.79–7.96%) (Table 3). All mafic-ultramafic intrusive rocks and diorites in the fault zone show minor LREE enriched patterns and minor Eu anomalies with Eu/Eu* ratios of 0.61–1.25 (Fig. 8). On primitive mantle–normalized plots, the investigated samples display enrichment in Th, Pb and variable depletion in high field strength elements (HFSE) such as Nb, Ta, Zr, Hf, Ti and Rb (Fig. 8). The andesitic porphyrite and basalt samples from the Shuangxiwu Group show features that are similar to those within the fault zone (Fig. 9, 10). The andesitic porphyrite samples (1468 and 1468-1) have $SiO_2$ content of 60.4~67.6 %, CaO of 0.05~1.31 %, $Na_2O$ of 1.65~5.42 % and $K_2O$ of 1.09~7.73 %, with $K_2O/Na_2O$ of 0.2 to 4.68 (Table 3). The basalt sample (1467) from the Shuangxiwu Group in the Jiangnan belt displays a $SiO_2$ content of 50.02 %, CaO of 9.95 %, $Na_2O$ of 3.34 % and $K_2O$ of 1.15 %. The basaltic rocks and andesitic porphyrite samples yield LREE enriched patterns with minor depletion of Eu (Eu/Eu* ratios of 0.77~0.94). Depletion of Ti, Sr, Nb, Ta and enrichment of Rb, Th, Pb are also observed, similar to those from the fault zone at Shijiao (Fig. 8), trace element patterns from pyroclastic rock samples are also similar to those from the fault zone at Shijiao.

## 5. Discussion

### *5.1. Field geology, petrology and geochemistry*

Within the Jiangshan-Shaoxing fault zone at Shijiao, migmatized diorite intrudes the hornblende schist, and coarse-grained ultramafic rocks and gabbro occur as inclusions in the migmatized quartz diorite. Age data are consistent with field observations. The hornblende schist and mafic-ultramafic inclusions were generated at ca. 880 Ma (888 ± 10 Ma, K–Ar hornblende, Zhou and Zhu, 1992; 879 ± 10 Ma, LA-ICPMS U–Pb gabbro, Yao et al., 2014a), and is older than the formation of quartz diorite (ca. 850 Ma).

Rock units exposed to the northwest of the fault zone are the typical volcanic rocks of the Shuangxiwu Group (ca. 990~880 Ma), the lower part of which are intruded by 913~905 Ma I-type granitoids (Fig. 2; Ye et al., 2007; Li et al., 2009). On the other hand, the Chencai Complex of the Cathaysia Block is composed mainly of pelitic sedimentary rocks with minor mafic rocks and experienced Paleozoic metamorphism of amphibolite facies. Southeast-directed thrusts occur within the complex and are assumed to be Paleozoic, synchronous with metamorphism but have not been directly dated (Li et al., 2010).

Geochemical data suggests formation of rock units within the Jiangshan-Shaoxing fault zone at Shijiao area in a convergent plate margin setting. The migmatized quartz diorite samples show a depletion in high field strength elements (HFSE) such as Nb, Ta, Zr, Hf and Ti compared with their neighboring elements (Fig. 9), similar to those formed in an island arc setting (Wyman, 1999). Mafic-ultramafic intrusive rocks that occur as inclusions within the migmatized diorite also display similar geochemical features. Pyroclastic and basaltic rocks from the Shuangxiwu Group in the eastern Jiangnan belt likewise display geochemical signatures typical of a convergent plate margin setting (Fig. 9). On tectonic discrimination diagrams, such as Ti–Zr plot of Peace and Cann (1973), Y–La–Nb plot of Wood (1980) and Cr–Y plot of Pearce et al. (1982) (Fig. 10), most of the investigated samples plot in the field of arc basalts. The quartz diorite samples from the fault zone display obvious Nb–Ta depletion, which is indicative of volcanic arc geochemical signature, as well as the andesitic porphyrite from the Shuangxiwu Group. These features are comparable to those of the typical Shuangxiwu arc (Li et al., 2009). Thus, based on rock assemblages, field geology and geochemical data, we infer that the migmatized quartz diorite and mafic-ultramafic rocks caught within the Jiangshan-Shaoxing fault zone at Shijiao were generated in a convergent margin setting, similar to the protolith of the amphibolite schist in the studied area (Yao et al., 2014a) and also similar to rock units of the Shuangxiwu Group in the Jiangnan belt (Li et al., 2009).

### *5.2. Tectonic implications*

Geological, geochronological and geochemical features of rock units within the Jiangshan-Shaoxing fault zone in the Shijiao area include a suite of quartz diorite and meta-mafic-ultramafic rocks and hornblende schist with ages around 880-850 Ma, and a convergent plate margin magmatic arc geochemical signature. Furthermore, these features are comparable to those of the adjoining but lower greenschist facies metamorphic rocks of the Shuangxiwu Group, which is also interpreted as part of a ca.

1000-880 Ma magmatic arc (Shu and Charvet, 1996; Charvet et al., 1996; Chen et al., 2009; Li et al., 2009).

The subduction direction of oceanic crust between the Yangtze and Cathaysia blocks has generally been considered to be northwestward beneath the Jiangnan arc (also referred to as 'Shuangxiwu arc' or 'Huaiyu arc') in SE margin of the Yangtze Block (Shu and Charvet, 1996). The supra-subduction zone Northeast Jiangxi Ophiolite, which is exposed between an arc assemblage and the continental Yangtze Block, is suggested as a relic of the back-arc basin (Shu and Charvet, 1996; Li et al., 1997). The subduction direction of the back-arc basin in its latest stage has also been suggested to be northwestward as constrained by analysis of inferred ca. 930-900 Ma ductile deformation fabrics from areas in and adjacent the Northeast Jiangxi suture zone (Shu and Charvet, 1996). Recent work has also suggested the presence of Neoproterozoic southwestward subduction beneath the NE margin of the Cathaysia Block (Wang et al., 2014; Zhao, 2015). The arc type rock suites in the fault zone at Shijiao area, if they belong to the Cathaysia Block (cf. Shui et al., 1986; Li et al., 2010), could serve as the evidence of a magmatic arc on the northeastern margin of the Cathaysia Block related to southwestward-directed subduction beneath the margin. Thus, the affinity of the rock suites within the Jiangshan-Shaoxing fault zone can help constrain the number and direction of subduction zones associated with assembly of the Yangtze and Cathaysia blocks.

The ca. 880–850 Ma arc type rock units within Jiangshan-Shaoxing fault zone at Shijiao area indicate this area differs from the Chencai Complex. The complex has a protolith dominated by continental derived materials metamorphosed at ca. 426 Ma (Li et al., 2010), along with minor meta-mafic rocks which have yielded ages of ca. 858 Ma and ca. 438 Ma with the former displaying within plate geochemical affinities (Shu et al., 2011; Yao et al., 2014a). The amphibolite-grade metamorphism in the fault zone most likely reflects the proximity to the Cathaysia Block, which underwent widespread early Paleozoic metamorphism (Shu et al., 2014, 2015), as inferred from mylonitization dated at ca. 421–398 Ma (Ar-Ar, Shu et al., 1999). On the other hand, the ca. 1000-880 Ma arc type meta-magmatic rocks of the Shuangxiwu Group are similar to those within Jiangshan-Shaoxing fault zone at Shijiao. Moreover, given that the middle to late Neoproterozoic Sinian System and Heshangzheng Group unconformably overlie the Shuangxiwu Group and show little to no metamorphism and deformation (BGMRZJ, 1989), then the metamorphism and deformation of the Shuangxiwu Group must be Neoproterozoic. Therefore, the Paleozoic amphibolite facies metamorphism in the fault zone does not conflict with Neoproterozoic greenschist facies metamorphism of the eastern Jiangnan belt and with the mostly accepted NW-ward accretionary subduction beneath Jiangnan belt (Charvet et al., 1996; Shu and Charvet, 1996; Cawood et al., 2013).

In this study, we suggest the andesitic and mafic-ultramafic rocks within the Jiangshan-Shaoxing fault zone at Shijiao belong to the Jiangnan orogenic belt and were produced in a convergent plate margin at ca. 880–850 Ma (Fig. 11). These results indicate that the previously proposed ca. 980–880 Ma convergent plate margin setting in the eastern Jiangnan belt (Ye et al., 2007; Li et al., 2009) lasted at least to ca.

850 Ma and is consistent with the overall duration of the convergent plate margin geochemical signature preserved within the Jiangnan belt (Shu et al., 1994, 2006; Zhao and Cawood, 2012; Cawoodet al, 2013; Zhang et al., 2013; Yao et al., 2015). Data on the age and origin of S-type granites within the Jiangnan orogenic belt along with the overall Neoproterozoic stratigraphic sequence that includes deformed and metamorphosed older units and younger unconformably overlying little deformed and unmetamorphosed middle to late Neoproterozoic units, constrains final assembly of the Yangtze and Cathaysia blocks to sometime between ca. 850-810 Ma (e.g. Wang et al., 2007, 2012; Zhao and Cawood, 2012; Yao et al., 2014b).

We believe the lithologies within the Jiangshan-Shaoxing fault zone at Shijiao formed in a subduction zone setting and do not belong to the Cathaysia Block, and therefore cannot be used as indicators for southeastward subduction of oceanic crust beneath the NE margin of Cathaysia Block. The fault along the NE margin of Chencai Complex constitutes the boundary of Cathaysia Block and Jiangnan belt at Shijiao. Field, age and geochemical relationships of this study argue against models suggesting ca. 880 Ma collision and ca. 860 Ma rifting of the South China Craton (e.g. Li et al., 2008). Our data require a younger assembly age, at least after ca. 850 Ma and a marginal position for South China within the Rodinia supercontinent (Cawood et al., 2013; Wang et al., 2014).

## 6. Conclusions

The ca. 880~850 Ma quartz diorite, mafic-ultramafic rocks and hornblende schist identified from within the Jiangshan-Shaoxing fault zone at Shijiao area are indicative of a convergent plate margin setting. Lithology, structure, age data, geochemistry and metamorphic grade indicate the rocks units in Shijiao area display close affinity with the Jiangnan belt rather than the Cathaysia Block. The investigated rock units formed around 880~850 Ma in a convergent plate margin setting in the eastern Jiangnan belt and do not provide evidence for Neoproterozoic subduction of oceanic crust beneath the NE margin of the Cathaysia Block. The Jiangshan-Shaoxing fault zone at Shijiao marks the NE margin of the Chencai Complex of the Cathaysia Block and delineates the boundary between the block and the Jiangnan belt.

## Acknowledgements

Reviews by Dr. Sanzhong Li and Dr. Wenjiao Xiao are gratefully acknowledged. We also thank Dr. Y.H. Yang and J.Q. Wang for their help with zircon dating and Hf isotopic data collection. We acknowledge the financial support provided by the National Basic Research Program of China (973 Program, No. 2012CB416701), the National Natural Science Foundation of China (Nos. 41330208, 41572200, 41272226) and the Bureau of China Geological Survey (No. 1212011121064-01).

## References


BGMRZJ (Bureau of Geology and mineral Resources Jiangxi Province), 1989. Regional Geology of Jiangxi Province. Geology Publishing House, Beijing, 5–575 (In Chinese with English Abstract).

Blichert-Toft, J., Albarede, F., 1997. The Lu–Hf isotope geochemistry of chondrites and the evolution of the mantle–crust system. Earth and Planetary Science Letters 148, 243–258.

Cawood, P.A., Wang, Y.J., Xu, Y.J., Zhao, G.C., 2013. Locating South China in Rodinia and Gondwana: a fragment of Greater Indian Lithosphere? Geology 41(8), 903–906.

Charvet, J., Shu, L.S., Shi, Y.S., Guo, L.Z., Faure, M., 1996. The building of south China: collision of Yangtze and Cathaysia blocks, problems and tentative answers. Journal of Southeast Asian Earth Sciences 13 (3–5), 223–235.

Charvet, J., Shu, L.S., Faure, M., Choulet, F., Wang, B., Lu, H.F., Le Breton, N., 2010.Structural development of the Lower Paleozoic belt of South China: Genesis of an intracontinental orogen. Journal of Asian Earth Sciences 39, 309–330.

Chen, Z.H., Xing, G.F., Guo, K.Y., Dong, Y.G., Chen, R., Zeng, Y., Li, L.M., He, Z.Y., Zhao, L., 2009. Petrogenesis of the Pingshui keratophyre from Zhejiang: Zircon U–Pb age and Hf isotope constraints. Chinese Science Bulletin 54, 610–617 (in Chinese with English abstract).

Dong, S.W., Zhang, Y.Q., Gao, R., Su, J.B., Liu, M., Li, J.H., 2015. A possible buried Paleoproterozoic collisional orogen beneath central South China: Evidence from seismic-reflection profiling. Precambrian Research 264, 1–10.

Li, X.H., Zhao, J.X., McCulloch, M.T., Zhou, G.Q., Xing, F.M., 1997. Geochemical and Sm-Nd isotopic study of Neoproterozoic ophiolites from southeastern China: petrogenesis and tectonic implications. Precambrian Research 81, 129-144.

Li, X.H, Li, W.X., Li, Z.X., Lo, C.H., Wang, J., Ye, M.F., Yang, Y.H., 2009. Amalgamation between the Yangtze and Cathaysia Blocks in South China: Constraints from SHRIMP U–Pb zircon ages, geochemistry and Nd–Hf isotopes of the Shuangxiwu volcanic rocks. Precambrian Research 174, 117–128.

Li, Z.X., Bogdanova, S.V., Collins, A.S., Davidson, A., De Waele, B., Ernst, R.E., Fitzsimons, I.C.W., Fuck, R.A., Gladkochub, D.P., Jacobs, J., Karlstrom, K.E., Lu, S., Natapov, L.M., Pease, V., Pisarevsky, S.A., Thrane, K., Vernikovsky, V., 2008. Assembly, configuration, and break-up history of Rodinia: a synthesis. Precambrian Research 160, 179–210.

Li, Z.X., Li, X.H., Wartho, J.A., Clark, C., Li, W.X., Zhang, C.L., Bao, C.M., 2010. Magmatic and metamorphic events during the early Paleozoic Wuyi□Yunkai orogeny, southeastern South China: New age constraints and pressure-temperature conditions. Geological Society of America Bulletin 122 (516), 772–793.

Ludwig, K.R., 2003. Isoplot 3.00, a geochronological Toolkit for Microsoft Excel. Berkeley Geochronology Center, Special Publication 4, 1-70.

McDonough, W.F., Sun, S.S., 1995. Composition of the Earth. Chemical Geology 120, 223-253.

Mullen, E.D., 1983. MnO/TiO2/P2O5—a minor element discriminant for basaltic rocks of oceanic environments and implication for petrogenesis. Earth Planet Science Letters 62, 53–62.

Pearce, J.A., Cann, J.R., 1973. Tectonic setting of basic volcanic rocks determined using trace element analyses. Earth and Planetary Science Letters 19, 290-300.

Pearce, J.A., 1982. Trace element characteristics of lavas from destructive plate boundaries. In: Thorpe, R.S. (Ed.), Andesites. Wiley, New York, pp. 525–548.

Pearce, J.A., Harris, N.B.W., Tindle, A.G., 1984. Trace element discrimination dia-grams for the tectonic interpretation of granitic rocks. Journal of Petrology 25,956–983.

Scherer, E., Munker, C., Mezger, K, 2001. Calibration of the Lutetium–Hafnium clock. Science 293, 683–687.

Shu, L.S., 2006. Predevonian Tectonic Evolution of South China: from Cathaysian Block to Caledonian Period Folded Orogenic Belt. Geological Journal of China Universities 12(4), 418-431. (In Chinese with English abstract)

Shu, L.S., 2012. An analysis of principal features of tectonic evolution in South China Block. Geological Bulletin of China 31(7), 1035-1053.

Shu, L.S., Zhou, G.Q., Shi, Y.S., Yin, J., 1994. Study on the high pressure metamorphic blueschist and its Late Proterozoic age in the Eastern Jiangnan belt. Chinese Science Bulletin 39, 1200–1204.

Shu, L.S., Charvet, J., 1996. Kinematics and geochronology of the Proterozoic Dongxiang - Shexian ductile shear zone: with HP metamorphism and ophiolitic melange (Jiangnan region, South China). Tectonophysics 267, 291–302.

Shu, L.S., Lu, H.F., Jia, D., Charvet, J., Faure, M., 1999, Study of the 40Ar/39Ar isotopic age for the early Paleozoic tectonothermal event in the Wuyishan region, South China. Journal of Nanjing University (Natural Science) 35(6), 668-674 (In Chinese with English abstract).

Shu, L.S., Faure, M., Jioang, S.Y., Yang, Q., Wang Y.J., 2006. SHRIMP zircon U-Pb age, litho- and biostratigraphic analyses of the Huaiyu Domain in South China - Evidence for a Neoproterozoic orogen, not Late Paleozoic-Early Mesozoic collision. Episodes 29(4), 244-252.

Shu, L.S., Faure, M., Yu, J.H., Jahn, B.M., 2011. Geochronological and geochemical features of the Cathaysia Block (South China): New evidence for the Neoproterozoic breakup of Rodinia.

Precambrian Research 187 (3–4), 263–276.

Shu, L.S., Jahn, B.M., Charvet, J., Santosh, M., Wang, B., Xu, X.S., and Jiang, S.Y., 2014. Early Paleozoic depositional environment and intracontinental orogeny in the Cathaysia Block (South China): implications from stratigraphic, structural, geochemical and geochronologic evidence. American Journal of Science 314, 154-186.

Shu, L., Wang, B., Cawood, P. A., Santosh, M., Xu, Z.Q., 2015. Early Paleozoic and early Mesozoic intraplate tectonic and magmatic events in the Cathaysia Block, South China. Tectonics 34, 1600-1621.

Shui, T., Xu, B.T., Liang, R.H., Qiu, Y.S., 1986. Shaoxing-Jiangshan deep-seated fault zone, Zhejiang Province. Chinese Science Bulletin 31(18), 1250–1255.

Sun, S.S., McDonough, W.F., 1989. Chemical and isotopic systematics of oceanic basalts: implication for mantle composition and processes. In: Saunder, A.D., Norry, M.J. (Eds.), Magmatism in the Ocean Basins: Geological Society, London, Special Publications 42, 313–345.

Wang, J., Deng, Q., Wang, Z. J., 2013a. New evidence for sedimentary attributes and timing of the “Macaoyuan Group conglomerates” on the northern margin of the Yangtze block in southern China. Precambrian Research 235, 58-70.

Wang, W., Zhou, M.F., Yan, D.P., Li, J.W., 2012. Depositional age, provenance, and tectonic setting of the Neoproterozoic Sibao Group, southeastern Yangtze Block, South China. Precambrian Research 192–195, 107–124.

Wang, X.L., Zhou, J.C., Griffin, W.L., Wang, R.C., Qiu, J.S., O’Reilly, S.Y., Xu, X.S., Liu, X.M., Zhang, G.L., 2007. Detrital zircon geochronology of Precambrian basement sequences in the

Jiangnan orogen: Dating the assembly of the Yangtze and Cathaysia Blocks. Precambrian Research 159, 117–131.

Wang, Y.J., Zhang, A.M., Cawood, P.A., Fan, W.M., Xu, J.F., Zhang, G.W., Zhang, Y.Z., 2013b. Geochronological, geochemical and Nd-Hf-Os isotopic fingerprinting of an early Neoproterozoic arc-back-arc system in South China and its accretionary assembly along the margin of Rodinia. Precambrian Research 231, 343–371.

Wang, Y.J., Zhang, Y.Z., Fan, W.M., Geng, H.Y., Zou, H.P., Bi, X.W., 2014. Early Neoproterozoic accretionary assemblage in the Cathaysia block: geochronological, Lu–Hf isotopic and geochemical evidence from granitoid gneisses. Precambrian Research 249, 144–161.

Wyman, D. A., 1999. A 2.7 Ga depleted tholeiite suite: evidence of plume-arc interaction in the Abitibi Greenstone belt, Canada. Precambrian Research 97, 27–42.

Wood, D.A., 1980. The application of a Th–Hf–Ta diagram to problems of tecto-magmatic classification and to establishing the nature of crustal contamination of basaltic lavas of the British Tertiary volcanic province. Earth Planet Science Letters 50, 11–30.

Yao, J.L., Shu, L.S., Santosh, M., Li, J.Y., 2013. Geochronology and Hf isotope of detrital zircons from Precambrian sequences in the eastern Jiangnan Orogen: Constraining the assembly of Yangtze and Cathaysia Blocks in South China. Journal of Asian Earth Sciences 74, 225–243.

Yao, J.L., Shu, L.S., Santosh, M., Xu, Z.Q., 2014a. Palaeozoic metamorphism of the Neoproterozoic basement in NE Cathaysia: zircon U–Pb ages, Hf isotope and whole-rock geochemistry from the Chencai Group. Journal of the Geological Society, London 171, 281–297.

Yao, J.L, Shu, L.S., Santosh, M., Zhao, G.C., 2014b. Neoproterozoic arc-related mafic-ultramafic rocks and syn-collision granite from the western segment of the Jiangnan Orogen, South China: constraints on the Neoproterozoic assembly of the Yangtze and Cathaysia Blocks. Precambrian Research 243, 39– 62.

Yao, J.L., Shu, L.S., Santosh, M., Li, J.Y., 2015. Neoproterozoic arc-related andesite and orogeny-related unconformity in the eastern Jiangnan orogenic belt: Constraints on the assembly of the Yangtze and Cathaysia blocks in South China. Precambrian Research 262, 84–100.

Ye, M.F., Li, X.H., Li, W.X., Liu, Y., Li, Z.X., 2007. SHRIMP zircon U–Pb geochronological and whole-rock geochemical evidence for an early Neoproterozoic Sibaoan magmatic arc along the southeastern margin of the Yangtze Block. Gondwana Research 12, 144–156.

Zhang, B.T., Ling, H.F., Shen,W.Z., Liu, J.S., Yang, J.D., Tao, X.C., 1990. Sm–Nd isochronic age of spilite-keratophyre of Shuangxiwu Group in Xiqiu, Shaoxing, Zhejiang Province. Journal of Nanjing University (Earth Science) 2, 9–14 (in Chinese with English Abstract).

Zhang, Y.Z., Wang, Y.J., Geng, H.Y., Zhang, Y.H., Fan, W.M., Zhong, H., 2013. Early Neoproterozoic (850 Ma) back-arc basin in the Central Jiangnan Orogen (Eastern South China): Geochronological and petrogenetic constraints from meta-basalts. Precambrian Research 231, 325-342.

Zhao, G.C., 2015. Jiangnan Orogen in South China: Developing from divergent double subduction. Gondwana Research 27(3), 1173–1180.

Zhao, G.C., Cawood, P.A., 2012. Precambrian geology of China. Precambrian Research 222–223, 13–54.

Zhao, G.C. Sun, D.Y., 1994. The studies on metamorphic stages and metamorphic PTD path of Chencai Group, southwestern Zhejiang province. Journal of Changchun University of Earth Sciences 24(3), 246-253 (In Chinese with English abstract).

Zhou, X.M., Zhu, Y.H., Chen, J.G., 1993. Discovering of nodule ultramafic rocks and it's genesis. Chinese Science Bulletin, 604-604.

Zhou X M, Zhu Y H., 1992. Magma mixing in the Jiang-Shao fault zone and the Precambrian geology of both side of the Jiang-Shao zone (in Chinese with English abstract). Science in China Series B 22, 298–303.

Zhu, Y.H., Zhou, X.M., 1994. Mylonitization of diorite in Jiangshao fracture belt Zhejiang province. Chinese Journal of Geochemistry 13(4), 371-378.

## Captions of figures

Fig.1. Geological sketch map of the Jiangnan orogen, South China Craton (1: Jiangshan-Shaoxing fault; 2: Zhenghe-Dapu fault; 3: Northeast Jiangxi fault; 4: Jiujiang-Shitai fault; 5: Tanlu fault; SECCLMVZ: Southeast China costal late Mesozoic volcanic zone).

Fig.2. Geological sketch map of the Jiangshan-Shaoxing fault zone at Shijiao area, South China (Pt3sh: Shuangxiwu Group; Pt3h: Heshangzheng Group; Pt3z: Sinian System; Pt3ch: Chencai Complex).

Fig.3 Cross sections with sample locations.

Fig.4. Representative field photos of samples analyzed in this study. (A) Field photograph of the andesitic porphyrite sample 1468. (B) Field photograph showing the location of quartz diorite sample 1194. (C) Filed photograph of bedded chert. (D) Field photograph of the dunite within gabbro. (E) Field photograph of volcanic sedimentary rock sample 1470. (F) Field photograph showing the location of hornblende schist.

Fig.5. Photomicrographs of samples analyzed in this study. (A) Thin section

photomicrograph of amphibole pyroxenite sample 1472-11 (crossed nicols). (B) Thin section photomicrograph of sample 1472-05 (crossed nicols). (C) Photomicrograph of gabbro sample 1472-18 (crossed nicols). (D) Thin section photomicrograph of amphibole pyroxenite sample 1472-11 (crossed nicols). (E) Photomicrograph of quartz diorite sample 1194 (crossed nicols). (F) Photomicrograph of hornblende schist (crossed nicols). Qz, quartz; Mus, Muscovite; Cpx, clinopyroxene; Ol, olivine; Plag, plagioclase; HB, hornblende.

Fig.6. U–Pb concordia plots for zircons from quartz diorite and gabbro from the Jiangshan-Shaoxing fault zone at Shijiao area, South China Craton.

Fig.7. A: Plot of εHf(t) vs. zircon U–Pb ages for the quartz diorite; B: Histogram of zircon Hf model ages for the quartz diorite.

Fig.8. Zr/TiO2 vs Nb/Y diagram of analyzed mafic samples in this study.

Fig.9. (a), Chondrite-normalized REE patterns for analyzed samples (normalization values are from Sun and McDonough (1989); (b) Primitive mantle-normalized incompatible element distribution spider-grams for analyzed samples. The normalization values are from McDonough and Sun (1995).

Fig.10. (a), Plot of Ti–Zr for gabbro samples (after Pearce, and Cann, 1973). (b), Th–Hf–Ta diagram (after Wood, 1980) for the samples from Shijiao area (c), Plot of Cr–Y for analyzed samples (after Mullen, 1983). (d) Plot of Rb–(Y+Nb) for quartz diorite samples (after Pearce et al., 1984).

Fig. 11. Tectonic evolution model for the eastern Jiangshan-Shaoxing suture zone, South China.

## Captions of tables

Table 1 U-Pb data for zircons in gabbro and quartz diorite from the eastern Jiangshan-Shaoxing fault zone at Shijiao, South China Craton.

Table 2 Hf isotope analyses for zircons in gabbro and quartz diorite from the eastern Jiangshan-Shaoxing fault zone at Shijiao, South China Craton.

Table 3 Major and trace element data for representative samples from the eastern Jiangshan-Shaoxing fault zone at Shijiao, South China Craton.

**Table 1 U-Pb data for zircons in gabbro from the Shijiao area within the eastern Jiangshan-shaoxing fault zone**

| Analysis | CORRECTED RATIOS | | | | | | CORRECTED AGES (Ma) | | | | | | Th/U ratios | concor-dance |
|---|---|---|---|---|---|---|---|---|---|---|---|---|---|---|
| | 207Pb/206Pb | 1s | 207Pb/235U | 1s | 206Pb/238U | 1s | 207Pb/206Pb | 1s | 207Pb/235U | 1s | 206Pb/238U | 1s | | |
| **Sample 1194: Quartz diortie from the eastern Jiangshan-Shaoxing fault zone at Shijiao** | | | | | | | | | | | | | | |
| 1155-01 | 0.060790 | 0.001700 | 1.253290 | 0.034040 | 0.149550 | 0.002290 | 632 | 62 | 825 | 15 | 898 | 13 | 1.06 | 109 |
| 1155-02 | 0.067630 | 0.001370 | 1.318450 | 0.025820 | 0.141410 | 0.002090 | 857 | 43 | 854 | 11 | 853 | 12 | 1.30 | 100 |
| 1155-03 | 0.067370 | 0.001140 | 1.314340 | 0.021600 | 0.141500 | 0.002020 | 849 | 36 | 852 | 9 | 853 | 11 | 0.86 | 100 |
| 1155-04 | 0.067330 | 0.001020 | 1.318810 | 0.019670 | 0.142070 | 0.001970 | 848 | 32 | 854 | 9 | 856 | 11 | 0.88 | 100 |
| 1155-05 | 0.067570 | 0.001420 | 1.319310 | 0.026870 | 0.141620 | 0.002100 | 855 | 45 | 854 | 12 | 854 | 12 | 0.97 | 100 |
| 1155-06 | 0.068270 | 0.001000 | 1.335020 | 0.019260 | 0.141850 | 0.001970 | 877 | 31 | 861 | 8 | 855 | 11 | 1.34 | 99 |
| 1155-07 | 0.067250 | 0.001310 | 1.317230 | 0.024680 | 0.142080 | 0.002080 | 846 | 41 | 853 | 11 | 856 | 12 | 0.90 | 100 |
| 1155-08 | 0.067510 | 0.002220 | 1.326200 | 0.041670 | 0.142480 | 0.002440 | 854 | 70 | 857 | 18 | 859 | 14 | 1.38 | 100 |
| 1155-09 | 0.067310 | 0.002390 | 1.314460 | 0.043980 | 0.141660 | 0.002700 | 847 | 76 | 852 | 19 | 854 | 15 | 1.01 | 100 |
| 1155-10 | 0.067300 | 0.001550 | 1.317440 | 0.029350 | 0.141990 | 0.002130 | 847 | 49 | 853 | 13 | 856 | 12 | 1.03 | 100 |
| 1155-11 | 0.067570 | 0.001730 | 1.321280 | 0.031940 | 0.141850 | 0.002270 | 855 | 54 | 855 | 14 | 855 | 13 | 1.07 | 100 |
| 1155-12 | 0.067520 | 0.001650 | 1.322180 | 0.030840 | 0.142050 | 0.002170 | 854 | 52 | 855 | 13 | 856 | 12 | 1.30 | 100 |
| 1155-13 | 0.067520 | 0.001770 | 1.318230 | 0.032750 | 0.141620 | 0.002270 | 854 | 56 | 854 | 14 | 854 | 13 | 1.15 | 100 |
| 1155-14 | 0.074230 | 0.005220 | 1.528950 | 0.102560 | 0.149430 | 0.004050 | 1048 | 146 | 942 | 41 | 898 | 23 | 1.38 | 95 |
| 1155-15 | 0.067560 | 0.001640 | 1.318900 | 0.030390 | 0.141620 | 0.002210 | 855 | 52 | 854 | 13 | 854 | 12 | 1.29 | 100 |
| 1155-16 | 0.067330 | 0.000770 | 1.315830 | 0.014990 | 0.141770 | 0.001860 | 848 | 24 | 853 | 7 | 855 | 11 | 1.06 | 100 |
| 1155-17 | 0.066590 | 0.001200 | 1.300060 | 0.022790 | 0.141630 | 0.001960 | 825 | 38 | 846 | 10 | 854 | 11 | 1.18 | 101 |
| 1155-18 | 0.067010 | 0.001740 | 1.304350 | 0.032420 | 0.141210 | 0.002210 | 838 | 55 | 848 | 14 | 852 | 12 | 1.20 | 100 |
| 1155-19 | 0.067000 | 0.001100 | 1.307450 | 0.020850 | 0.141570 | 0.001940 | 838 | 35 | 849 | 9 | 854 | 11 | 1.09 | 101 |
| 1155-20 | 0.067990 | 0.001700 | 1.322920 | 0.031580 | 0.141140 | 0.002190 | 868 | 53 | 856 | 14 | 851 | 12 | 0.93 | 99 |
| **Sample 1194-1: Quartz diorite from the eastern Jiangshan-Shaoxing fault zone at Shijiao** | | | | | | | | | | | | | | |
| 1155-1-01 | 0.067740 | 0.001710 | 1.331980 | 0.031810 | 0.142640 | 0.002280 | 861 | 54 | 860 | 14 | 860 | 13 | 1.29 | 100 |
| 1155-1-02 | 0.067660 | 0.001280 | 1.325740 | 0.023930 | 0.142140 | 0.002070 | 858 | 40 | 857 | 10 | 857 | 12 | 1.40 | 100 |
| 1155-1-03 | 0.067520 | 0.001010 | 1.322110 | 0.019240 | 0.142050 | 0.001940 | 854 | 32 | 855 | 8 | 856 | 11 | 1.33 | 100 |
| 1155-1-04 | 0.067430 | 0.001500 | 1.312700 | 0.027610 | 0.141230 | 0.002180 | 851 | 47 | 851 | 12 | 852 | 12 | 1.05 | 100 |
| 1155-1-05 | 0.067750 | 0.001510 | 1.316370 | 0.028120 | 0.140950 | 0.002120 | 861 | 47 | 853 | 12 | 850 | 12 | 1.22 | 100 |
| 1155-1-06 | 0.068190 | 0.001180 | 1.325200 | 0.021910 | 0.140980 | 0.002020 | 874 | 37 | 857 | 10 | 850 | 11 | 1.38 | 99 |
| 1155-1-07 | 0.067260 | 0.001320 | 1.310610 | 0.024490 | 0.141350 | 0.002080 | 846 | 42 | 850 | 11 | 852 | 12 | 1.57 | 100 |
| 1155-1-08 | 0.067620 | 0.001160 | 1.320360 | 0.021990 | 0.141640 | 0.001960 | 857 | 36 | 855 | 10 | 854 | 11 | 1.11 | 100 |
| 1155-1-09 | 0.067360 | 0.001190 | 1.312410 | 0.022410 | 0.141330 | 0.001980 | 849 | 38 | 851 | 10 | 852 | 11 | 1.29 | 100 |
| 1155-1-10 | 0.067340 | 0.000950 | 1.313360 | 0.018020 | 0.141490 | 0.001920 | 848 | 30 | 852 | 8 | 853 | 11 | 1.53 | 100 |
| 1155-1-11 | 0.067710 | 0.000690 | 1.341040 | 0.014130 | 0.143670 | 0.001890 | 860 | 22 | 864 | 6 | 865 | 11 | 0.75 | 100 |
| 1155-1-12 | 0.067850 | 0.001870 | 1.344810 | 0.035900 | 0.143770 | 0.002240 | 864 | 59 | 865 | 16 | 866 | 13 | 0.96 | 100 |
| 1155-1-13 | 0.067850 | 0.001340 | 1.340490 | 0.025960 | 0.143300 | 0.002030 | 864 | 42 | 863 | 11 | 863 | 11 | 1.32 | 100 |
| 1155-1-14 | 0.069740 | 0.002290 | 1.351100 | 0.042490 | 0.140530 | 0.002390 | 921 | 69 | 868 | 18 | 848 | 14 | 1.29 | 98 |
| 1155-1-15 | 0.068650 | 0.002250 | 1.350820 | 0.042840 | 0.142740 | 0.002310 | 888 | 69 | 868 | 19 | 860 | 13 | 0.90 | 99 |
| 1155-1-16 | 0.067590 | 0.001670 | 1.337430 | 0.032260 | 0.143540 | 0.002130 | 856 | 53 | 862 | 14 | 865 | 12 | 1.03 | 100 |
| 1155-1-17 | 0.068210 | 0.001520 | 1.333790 | 0.029110 | 0.141840 | 0.002060 | 875 | 47 | 861 | 13 | 855 | 12 | 1.05 | 99 |
| 1155-1-18 | 0.067320 | 0.000900 | 1.331500 | 0.017900 | 0.143470 | 0.001920 | 848 | 28 | 860 | 8 | 864 | 11 | 1.20 | 100 |
| 1155-1-19 | 0.067800 | 0.001540 | 1.337150 | 0.029920 | 0.143060 | 0.002040 | 862 | 48 | 862 | 13 | 862 | 12 | 1.22 | 100 |
| 1155-1-20 | 0.067860 | 0.001560 | 1.336220 | 0.029890 | 0.142830 | 0.002080 | 864 | 49 | 862 | 13 | 861 | 12 | 0.94 | 100 |
| **Sample 1472: Gabbro from the eastern Jiangshan-Shaoxing fault zone at Shijiao** | | | | | | | | | | | | | | |
| 1472-02 | 0.06821 | 0.0019 | 1.33354 | 0.03703 | 0.14182 | 0.00222 | 875 | 59 | 860 | 16 | 855 | 13 | 0.92 | 101 |
| 1472-03 | 0.06899 | 0.00127 | 1.43988 | 0.02782 | 0.15139 | 0.0021 | 898 | 39 | 906 | 12 | 909 | 12 | 0.97 | 100 |
| 1472-04 | 0.06841 | 0.00075 | 1.3402 | 0.01787 | 0.1421 | 0.00181 | 881 | 23 | 863 | 8 | 857 | 10 | 0.95 | 101 |
| 1472-05 | 0.07175 | 0.00346 | 1.50978 | 0.07018 | 0.15263 | 0.0032 | 979 | 101 | 934 | 28 | 916 | 18 | 0.66 | 102 |
| 1472-06 | 0.06887 | 0.0038 | 1.3581 | 0.07175 | 0.14303 | 0.00335 | 895 | 117 | 871 | 31 | 862 | 19 | 0.90 | 101 |
| 1472-07 | 0.06662 | 0.00138 | 1.30385 | 0.02801 | 0.14196 | 0.00199 | 826 | 44 | 847 | 12 | 856 | 11 | 3.39 | 99 |
| 1472-08 | 0.06763 | 0.00211 | 1.314 | 0.0404 | 0.14093 | 0.00231 | 857 | 66 | 852 | 18 | 850 | 13 | 0.83 | 100 |
| 1472-10 | 0.06976 | 0.00113 | 1.46442 | 0.02547 | 0.15228 | 0.00206 | 921 | 34 | 916 | 10 | 914 | 12 | 1.30 | 100 |
| 1472-11 | 0.06762 | 0.00076 | 1.30827 | 0.0177 | 0.14035 | 0.0018 | 857 | 24 | 849 | 8 | 847 | 10 | 1.34 | 100 |
| 1472-12 | 0.06795 | 0.00076 | 1.32689 | 0.01785 | 0.14165 | 0.00181 | 867 | 24 | 858 | 8 | 854 | 10 | 1.10 | 100 |
| 1472-16 | 0.06799 | 0.00171 | 1.34935 | 0.03423 | 0.14396 | 0.00216 | 868 | 53 | 867 | 15 | 867 | 12 | 1.23 | 100 |
| 1472-17 | 0.06779 | 0.00387 | 1.33085 | 0.07307 | 0.1424 | 0.00337 | 862 | 122 | 859 | 32 | 858 | 19 | 1.11 | 100 |
| 1472-18 | 0.06707 | 0.0021 | 1.33877 | 0.04135 | 0.14479 | 0.00239 | 840 | 67 | 863 | 18 | 872 | 13 | 1.62 | 99 |
| 1472-19 | 0.06734 | 0.00092 | 1.32629 | 0.02057 | 0.14286 | 0.00189 | 848 | 29 | 857 | 9 | 861 | 11 | 0.96 | 100 |
| 1472-20 | 0.06813 | 0.00133 | 1.33154 | 0.02717 | 0.14176 | 0.00201 | 873 | 41 | 860 | 12 | 855 | 11 | 0.92 | 101 |
| 1472-21 | 0.06778 | 0.00101 | 1.33643 | 0.02217 | 0.14301 | 0.00192 | 862 | 32 | 862 | 10 | 862 | 11 | 1.25 | 100 |
| 1472-22 | 0.06902 | 0.0017 | 1.34383 | 0.03337 | 0.14123 | 0.00215 | 899 | 52 | 865 | 14 | 852 | 12 | 0.91 | 102 |
| 1472-23 | 0.06899 | 0.00236 | 1.36084 | 0.04566 | 0.14308 | 0.0025 | 898 | 72 | 872 | 20 | 862 | 14 | 1.09 | 101 |
| 1472-24 | 0.06751 | 0.00398 | 1.32901 | 0.07533 | 0.14279 | 0.00345 | 854 | 126 | 858 | 33 | 860 | 19 | 0.92 | 100 |
| 1472-25 | 0.06781 | 0.00126 | 1.33105 | 0.02607 | 0.14238 | 0.00199 | 863 | 39 | 859 | 11 | 858 | 11 | 0.95 | 100 |
| 1472-26 | 0.0694 | 0.00198 | 1.36733 | 0.03906 | 0.14293 | 0.00234 | 911 | 60 | 875 | 17 | 861 | 13 | 1.10 | 102 |
| 1472-27 | 0.06972 | 0.00146 | 1.39221 | 0.03038 | 0.14487 | 0.00215 | 920 | 44 | 886 | 13 | 872 | 12 | 1.26 | 102 |
| 1472-28 | 0.06926 | 0.00143 | 1.37675 | 0.02982 | 0.1442 | 0.00213 | 906 | 44 | 879 | 13 | 868 | 12 | 0.99 | 101 |
| 1472-29 | 0.06846 | 0.00114 | 1.36304 | 0.02499 | 0.14443 | 0.00204 | 883 | 35 | 873 | 11 | 870 | 11 | 0.84 | 100 |
| 1472-30 | 0.06839 | 0.00231 | 1.36982 | 0.0456 | 0.14531 | 0.00256 | 880 | 72 | 876 | 20 | 875 | 14 | 1.17 | 100 |
| 1472-31 | 0.0686 | 0.00084 | 1.34523 | 0.01997 | 0.14226 | 0.00192 | 887 | 26 | 865 | 9 | 857 | 11 | 2.04 | 101 |
| 1472-32 | 0.06862 | 0.00177 | 1.34143 | 0.03508 | 0.14182 | 0.00223 | 887 | 55 | 864 | 15 | 855 | 13 | 1.14 | 101 |
| 1472-33 | 0.06984 | 0.00163 | 1.43484 | 0.03427 | 0.14905 | 0.00229 | 924 | 49 | 904 | 14 | 896 | 13 | 1.46 | 101 |

**Table 2 Hf isotope analyses for zircons in gabbro and quartz diorite from the eastern Jiangshan-Shaoxing fault zone at Shijiao**

| Sample | 176Yb/177 | 2σ | 176Lu/177 | 2σ | 176Hf/177 | 2σ | εHf(t) | εHf(0) | t | λ | T1 (Ma | T2 (Ma | fLu/Hf |
|---|---|---|---|---|---|---|---|---|---|---|---|---|---|
| **Sample 1194: Quartz diorite from the eastern Jiangshan-Shaoxing fault zone at Shijiao** | | | | | | | | | | | | | |
| 1194-01 | 0.036205 | 0.000145 | 0.000608 | 0.000001 | 0.282555 | 0.00 | 11.80 | -7.69 | 898 | 2.E-11 | 978 | 1027 | -0.98 |
| 1194-02 | 0.066593 | 0.002380 | 0.001230 | 0.000061 | 0.282541 | 0.00 | 9.99 | -8.16 | 853 | 2.E-11 | 1013 | 1107 | -0.96 |
| 1194-03 | 0.022836 | 0.000061 | 0.000417 | 0.000002 | 0.282558 | 0.00 | 11.05 | -7.56 | 853 | 2.E-11 | 968 | 1039 | -0.99 |
| 1194-04 | 0.024684 | 0.000055 | 0.000440 | 0.000002 | 0.282552 | 0.00 | 10.89 | -7.77 | 856 | 2.E-11 | 977 | 1052 | -0.99 |
| 1194-05 | 0.033575 | 0.000232 | 0.000611 | 0.000003 | 0.282503 | 0.00 | 9.00 | -9.52 | 854 | 2.E-11 | 1050 | 1171 | -0.98 |
| 1194-06 | 0.051787 | 0.000209 | 0.000968 | 0.000001 | 0.282551 | 0.00 | 10.53 | -7.81 | 855 | 2.E-11 | 992 | 1074 | -0.97 |
| 1194-07 | 0.052784 | 0.000501 | 0.000916 | 0.000004 | 0.282537 | 0.00 | 10.08 | -8.31 | 856 | 2.E-11 | 1010 | 1103 | -0.97 |
| 1194-08 | 0.032453 | 0.000088 | 0.000580 | 0.000000 | 0.282518 | 0.00 | 9.65 | -9.00 | 859 | 2.E-11 | 1028 | 1133 | -0.98 |
| 1194-09 | 0.042549 | 0.000901 | 0.000742 | 0.000011 | 0.282487 | 0.00 | 8.35 | -10.09 | 854 | 2.E-11 | 1076 | 1212 | -0.98 |
| 1194-10 | 0.042784 | 0.000718 | 0.000707 | 0.000007 | 0.282540 | 0.00 | 10.29 | -8.22 | 856 | 2.E-11 | 1001 | 1090 | -0.98 |
| 1194-11 | 0.035768 | 0.000179 | 0.000604 | 0.000001 | 0.282573 | 0.00 | 11.51 | -7.04 | 855 | 2.E-11 | 952 | 1012 | -0.98 |
| 1194-12 | 0.031824 | 0.000308 | 0.000522 | 0.000007 | 0.282518 | 0.00 | 9.63 | -8.99 | 856 | 2.E-11 | 1027 | 1132 | -0.98 |
| 1194-13 | 0.038055 | 0.000454 | 0.000638 | 0.000004 | 0.282511 | 0.00 | 9.26 | -9.25 | 854 | 2.E-11 | 1040 | 1154 | -0.98 |
| 1194-14 | 0.029944 | 0.000285 | 0.000523 | 0.000002 | 0.282440 | 0.00 | 7.81 | -11.72 | 898 | 2.E-11 | 1134 | 1280 | -0.98 |
| 1194-15 | 0.041834 | 0.000441 | 0.000679 | 0.000011 | 0.282482 | 0.00 | 8.23 | -10.25 | 854 | 2.E-11 | 1080 | 1219 | -0.98 |
| **Sample 1194-1: Quartz diorite from the eastern Jiangshan-Shaoxing fault zone at Shijiao** | | | | | | | | | | | | | |
| 1194-1-01 | 0.042618 | 0.000163 | 0.000686 | 0.000004 | 0.282524 | 0.00 | 9.84 | -8.77 | 860 | 2.E-11 | 1022 | 1122 | -0.98 |
| 1194-1-02 | 0.047503 | 0.000541 | 0.000779 | 0.000005 | 0.282541 | 0.00 | 10.34 | -8.15 | 857 | 2.E-11 | 1001 | 1088 | -0.98 |
| 1194-1-03 | 0.019452 | 0.000152 | 0.000370 | 0.000002 | 0.282481 | 0.00 | 8.40 | -10.30 | 856 | 2.E-11 | 1074 | 1210 | -0.99 |
| 1194-1-04 | 0.053640 | 0.000269 | 0.000940 | 0.000005 | 0.282522 | 0.00 | 9.45 | -8.84 | 852 | 2.E-11 | 1032 | 1140 | -0.97 |
| 1194-1-05 | 0.032485 | 0.000313 | 0.000592 | 0.000007 | 0.282472 | 0.00 | 7.82 | -10.62 | 850 | 2.E-11 | 1092 | 1242 | -0.98 |
| 1194-1-06 | 0.029102 | 0.000163 | 0.000554 | 0.000003 | 0.282474 | 0.00 | 7.91 | -10.55 | 850 | 2.E-11 | 1089 | 1236 | -0.98 |
| 1194-1-07 | 0.030517 | 0.000140 | 0.000553 | 0.000004 | 0.282421 | 0.00 | 6.09 | -12.41 | 852 | 2.E-11 | 1162 | 1353 | -0.98 |
| 1194-1-08 | 0.032824 | 0.000095 | 0.000581 | 0.000003 | 0.282529 | 0.00 | 9.95 | -8.58 | 854 | 2.E-11 | 1012 | 1110 | -0.98 |
| 1194-1-09 | 0.028154 | 0.000201 | 0.000517 | 0.000007 | 0.282426 | 0.00 | 6.30 | -12.22 | 852 | 2.E-11 | 1153 | 1340 | -0.98 |
| 1194-1-10 | 0.033464 | 0.000298 | 0.000577 | 0.000002 | 0.282378 | 0.00 | 4.57 | -13.94 | 853 | 2.E-11 | 1222 | 1450 | -0.98 |
| 1194-1-11 | 0.043960 | 0.000459 | 0.000715 | 0.000004 | 0.282536 | 0.00 | 10.35 | -8.35 | 865 | 2.E-11 | 1007 | 1093 | -0.98 |
| 1194-1-12 | 0.050065 | 0.000190 | 0.000801 | 0.000002 | 0.282504 | 0.00 | 9.18 | -9.49 | 866 | 2.E-11 | 1054 | 1168 | -0.98 |
| 1194-1-13 | 0.057981 | 0.000315 | 0.000938 | 0.000001 | 0.282515 | 0.00 | 9.44 | -9.09 | 863 | 2.E-11 | 1042 | 1149 | -0.97 |
| 1194-1-14 | 0.055306 | 0.000232 | 0.000942 | 0.000001 | 0.282552 | 0.00 | 10.42 | -7.78 | 848 | 2.E-11 | 990 | 1076 | -0.97 |
| 1194-1-15 | 0.037050 | 0.000419 | 0.000660 | 0.000006 | 0.282539 | 0.00 | 10.39 | -8.24 | 860 | 2.E-11 | 1001 | 1087 | -0.98 |

**Table 3 Major and trace element data for samples from the Shijiao area in the western Jiangnan orogenic belt**

| | 1305 | 1305-1 | 1306-1 | 1306-1-1 | 1306-2 | 1306-2-1 | 1411 | 1402 | 1402-1 | 1405 | 1405-1 | 1405-2 | 1405-3 | 1407 | 1409 | 1414 | 1414−1 | 1414−2 | 1414−3 |
|---|---|---|---|---|---|---|---|---|---|---|---|---|---|---|---|---|---|---|---|
| **Major elements (wt%)** | | | | | | | | | | | | | | | | | | | |
| SiO2 | 56.43 | 55.78 | 55.23 | 54.72 | 4.48 | 4.51 | 6.71 | 47.84 | 47.20 | 47.51 | 48.69 | 51.03 | 51.07 | 70.06 | 67.59 | 49.68 | 49.77 | 49.32 | 49.89 |
| TiO2 | 0.07 | 0.09 | 0.01 | 0.01 | 0.03 | 0.03 | 0.06 | 0.90 | 0.90 | 1.02 | 1.47 | 1.75 | 1.72 | 0.61 | 0.71 | 0.90 | 0.88 | 0.79 | 0.93 |
| Al2O3 | 3.58 | 3.56 | 0.48 | 0.45 | 0.71 | 0.73 | 1.64 | 12.26 | 12.13 | 15.29 | 13.80 | 14.32 | 14.25 | 14.62 | 15.79 | 16.19 | 16.20 | 15.21 | 16.63 |
| Fe2O3 | 1.23 | 1.34 | 0.27 | 0.27 | 3.37 | 3.37 | 0.60 | 10.67 | 10.68 | 8.89 | 9.94 | 10.90 | 10.87 | 4.15 | 5.45 | 10.04 | 10.04 | 10.51 | 10.04 |
| MnO | 0.00 | 0.00 | 0.01 | 0.01 | 0.13 | 0.13 | 0.04 | 0.14 | 0.14 | 0.12 | 0.15 | 0.16 | 0.16 | 0.11 | 0.12 | 0.19 | 0.19 | 0.14 | 0.21 |
| MgO | 31.45 | 31.42 | 30.51 | 30.30 | 20.90 | 20.74 | 19.26 | 13.31 | 13.28 | 7.77 | 6.50 | 7.04 | 6.96 | 1.44 | 1.75 | 8.61 | 8.64 | 8.86 | 8.41 |
| CaO | 0.17 | 0.23 | 3.46 | 3.43 | 28.03 | 27.92 | 28.76 | 8.49 | 8.42 | 7.08 | 7.81 | 6.02 | 5.97 | 1.04 | 0.59 | 6.39 | 6.42 | 8.17 | 4.82 |
| Na2O | 0.31 | 0.47 | 0.28 | 0.32 | 0.22 | 0.20 | 0.24 | 0.64 | 0.68 | 3.86 | 5.49 | 5.28 | 5.38 | 4.10 | 1.97 | 4.40 | 4.35 | 4.05 | 3.58 |
| K2O | 0.00 | 0.05 | 0.05 | 0.05 | 0.01 | 0.01 | 0.35 | 1.33 | 1.27 | 0.30 | 0.16 | 0.10 | 0.10 | 2.18 | 3.05 | 1.04 | 1.05 | 0.63 | 2.13 |
| P2O5 | 0.02 | 0.03 | 0.15 | 0.15 | 0.03 | 0.03 | 0.08 | 0.18 | 0.20 | 0.10 | 0.16 | 0.13 | 0.14 | 0.14 | 0.14 | 0.12 | 0.12 | 0.09 | 0.09 |
| LOI | 6.43 | 6.34 | 9.57 | 9.56 | 42.94 | 42.93 | 43.09 | 4.72 | 4.64 | 9.00 | 6.64 | 2.61 | 2.55 | 2.13 | 3.01 | 3.22 | 3.00 | 2.76 | 2.95 |
| TOTAL | 99.69 | 99.23 | 99.95 | 99.22 | 100.85 | 100.61 | 100.90 | 100.80 | 100.00 | 101.10 | 101.00 | 99.34 | 99.17 | 100.70 | 100.40 | 101.10 | 101.10 | 100.70 | 99.67 |
| Mg# | 98 | 98 | 100 | 100 | 93 | 92 | 71 | 71 | 64 | 57 | 56 | 56 | 41 | 39 | 98 | 63 | 63 | 63 | 63 |
| **Trace elements (ppm)** | | | | | | | | | | | | | | | | | | | |
| Li | 20.38 | 20.99 | 4.07 | 4.05 | 3.30 | 3.27 | 4.55 | 38.69 | 38.07 | 38.69 | 38.07 | 53.07 | 17.90 | 17.90 | 25.03 | 36.12 | 33.91 | 34.26 | 41.82 |
| Be | 0.24 | 0.31 | 0.24 | 0.20 | 0.11 | 0.12 | 0.74 | 0.70 | 0.67 | 0.70 | 0.67 | 0.72 | 1.02 | 1.52 | 1.84 | 0.71 | 0.29 | 0.73 | 0.88 |
| Sc | 2.65 | 2.96 | 1.76 | 1.85 | 1.79 | 1.71 | 1.04 | 16.16 | 17.82 | 16.16 | 17.82 | 27.08 | 33.08 | 9.62 | 12.96 | 29.47 | 25.59 | 31.15 | 34.39 |
| Ti | 603.2 | 554.9 | 275.7 | 269.6 | 109.7 | 88.24 | 87 | 5052 | 5036 | 5052 | 5036 | 5676 | 8296 | 3384 | 3923 | 5037 | 4443 | 5220 | 5986 |
| V | 27.98 | 25.75 | 12.44 | 13.04 | 6.82 | 6.36 | 0.71 | 214 | 221 | 214 | 221 | 106 | 185 | 42.62 | 52.16 | 122 | 111 | 126 | 258.5 |
| Cr | 35.89 | 21.59 | 14.97 | 15.34 | 11.15 | 8.46 | 11.87 | 630 | 627 | 630 | 627 | 282 | 168 | 46.32 | 72.65 | 282 | 363 | 287 | 299.2 |
| Mn | 41.06 | 31.34 | 1019 | 1055 | 89.43 | 82.32 | 237 | 1472 | 1462 | 1472 | 1462 | 1255 | 1558 | 1102 | 1303 | 2020 | 1538 | 2152 | 1631 |
| Co | 3.43 | 2.94 | 2.30 | 2.25 | 1.35 | 1.24 | 0.00 | 72.66 | 72.17 | 72.66 | 72.17 | 59.19 | 51.28 | 12.64 | 18.88 | 67.35 | 68.51 | 70.89 | 48.07 |
| Ni | 14.42 | 9.12 | 10.18 | 8.16 | 5.89 | 4.83 | 4.10 | 299 | 300 | 299 | 300 | 130 | 38.94 | 14.99 | 26.60 | 133 | 227 | 138 | 135.6 |
| Cu | 3.23 | 0.96 | 10.80 | 1.23 | 0.59 | 0.28 | 0.84 | 162 | 163 | 162 | 163 | 20.71 | 34.23 | 19.23 | 26.18 | 102 | 69.22 | 109 | 84.98 |
| Zn | 12.69 | 11.27 | 6.97 | 7.63 | 5.36 | 5.50 | 10.40 | 70.53 | 75.06 | 70.53 | 75.06 | 60.48 | 54.05 | 71.35 | 84.90 | 81.36 | 87.30 | 82.37 | 73.77 |
| Ga | 5.67 | 5.28 | 1.36 | 1.25 | 0.90 | 0.73 | 11.28 | 11.86 | 12.03 | 11.86 | 12.03 | 13.40 | 16.28 | 15.20 | 17.30 | 14.80 | 15.10 | 15.28 | 18.04 |
| Rb | 0.3 | 0.1 | 0.4 | 0.2 | 0.2 | 0.0 | 119.6 | 34.4 | 34.7 | 34.4 | 34.7 | 12.6 | 9.6 | 57.3 | 84.9 | 16.4 | 14.3 | 17.0 | 29.7 |
| Sr | 2.97 | 1.23 | 86.95 | 86.51 | 11.70 | 9.19 | 102 | 204 | 203 | 204 | 203 | 177 | 153 | 145 | 92.06 | 121 | 151 | 124 | 175.1 |
| Y | 1.01 | 0.81 | 3.70 | 3.67 | 1.12 | 1.05 | 0.56 | 16.26 | 16.40 | 16.26 | 16.40 | 19.54 | 26.12 | 32.73 | 31.61 | 22.30 | 14.55 | 23.12 | 19.08 |
| Zr | 30.47 | 29.94 | 12.79 | 13.05 | 5.73 | 4.63 | 4.92 | 96.07 | 95.98 | 96.07 | 95.98 | 70.26 | 111 | 226 | 215 | 83.65 | 67.76 | 88.70 | 104.1 |
| Nb | 1.67 | 1.56 | 0.96 | 0.81 | 0.34 | 0.21 | 0.72 | 9.91 | 9.90 | 9.91 | 9.90 | 3.37 | 5.11 | 11.40 | 13.45 | 4.55 | 2.34 | 3.62 | 3.62 |
| Mo | 0.23 | 0.06 | 0.60 | 0.64 | 0.07 | 0.10 | 0.09 | 0.50 | 0.47 | 0.50 | 0.47 | 0.10 | 0.12 | 0.28 | 0.23 | 0.22 | 0.18 | 0.19 | 0.24 |
| Cd | 0.05 | 0.07 | 0.07 | 0.07 | 0.04 | 0.05 | - | - | - | - | - | - | - | - | - | - | - | - | 0.22 |
| Sn | 0.82 | 0.36 | 0.21 | 0.19 | 0.11 | 0.10 | 1.35 | 1.79 | 1.75 | 1.79 | 1.75 | 1.33 | 0.54 | 1.63 | 2.33 | 0.98 | 0.92 | 1.54 | 1.04 |
| Cs | 0.50 | 0.41 | 0.14 | 0.11 | 0.67 | 0.69 | 2.57 | 0.88 | 0.90 | 0.88 | 0.90 | 2.43 | 11.18 | 4.82 | 5.60 | 1.75 | 2.52 | 1.79 | 3.85 |
| Ba | 3.11 | 0.84 | 9.88 | 5.64 | 1.22 | 0.76 | 471 | 468 | 463 | 468 | 463 | 129 | 56.41 | 635 | 467 | 285 | 202 | 330 | 825.6 |
| La | 4.56 | 4.52 | 2.79 | 2.26 | 0.46 | 0.34 | 1.44 | 15.09 | 14.81 | 15.09 | 14.81 | 6.75 | 8.20 | 26.79 | 29.96 | 11.70 | 5.16 | 12.03 | 9.49 |
| Ce | 9.36 | 9.14 | 6.39 | 5.60 | 1.26 | 0.98 | 2.37 | 30.12 | 26.99 | 30.12 | 26.99 | 18.42 | 22.73 | 54.55 | 60.29 | 27.35 | 14.09 | 28.08 | 21.60 |
| Pr | 0.88 | 0.88 | 0.79 | 0.68 | 0.17 | 0.14 | 0.30 | 3.18 | 3.12 | 3.18 | 3.12 | 2.00 | 2.55 | 6.85 | 7.38 | 2.63 | 1.52 | 2.66 | 2.65 |
| Nd | 2.82 | 2.86 | 3.22 | 2.74 | 0.79 | 0.63 | 0.92 | 13.43 | 13.14 | 13.43 | 13.14 | 9.57 | 12.42 | 27.09 | 28.91 | 11.46 | 7.25 | 11.69 | 11.10 |
| Sm | 0.34 | 0.33 | 0.73 | 0.63 | 0.22 | 0.18 | 0.18 | 2.83 | 2.79 | 2.83 | 2.79 | 2.56 | 3.30 | 5.12 | 5.49 | 2.72 | 1.87 | 2.77 | 2.68 |
| Eu | 0.04 | 0.04 | 0.22 | 0.19 | 0.06 | 0.05 | 0.69 | 0.98 | 0.95 | 0.98 | 0.95 | 1.05 | 1.06 | 1.31 | 1.28 | 0.86 | 0.72 | 0.88 | 0.98 |
| Gd | 0.23 | 0.21 | 0.67 | 0.64 | 0.24 | 0.23 | 0.18 | 2.76 | 2.73 | 2.76 | 2.73 | 2.64 | 3.36 | 4.84 | 5.28 | 2.83 | 1.97 | 2.89 | 3.09 |
| Tb | 0.03 | 0.02 | 0.09 | 0.09 | 0.03 | 0.03 | 0.03 | 0.45 | 0.44 | 0.45 | 0.44 | 0.49 | 0.63 | 0.78 | 0.86 | 0.51 | 0.36 | 0.51 | 0.44 |
| Dy | 0.17 | 0.16 | 0.66 | 0.61 | 0.20 | 0.20 | 0.20 | 2.55 | 2.53 | 2.55 | 2.53 | 2.94 | 3.86 | 4.52 | 5.07 | 3.18 | 2.22 | 3.21 | 3.15 |
| Ho | 0.04 | 0.04 | 0.13 | 0.13 | 0.04 | 0.04 | 0.04 | 0.47 | 0.47 | 0.47 | 0.47 | 0.55 | 0.73 | 0.91 | 1.00 | 0.63 | 0.42 | 0.64 | 0.71 |
| Er | 0.15 | 0.13 | 0.35 | 0.35 | 0.10 | 0.10 | 0.15 | 1.32 | 1.31 | 1.32 | 1.31 | 1.51 | 2.06 | 2.76 | 3.04 | 1.83 | 1.19 | 1.84 | 1.94 |
| Tm | 0.03 | 0.02 | 0.05 | 0.05 | 0.02 | 0.01 | 0.03 | 0.18 | 0.18 | 0.18 | 0.18 | 0.21 | 0.29 | 0.41 | 0.45 | 0.26 | 0.17 | 0.26 | 0.29 |
| Yb | 0.18 | 0.17 | 0.29 | 0.29 | 0.09 | 0.08 | 0.20 | 1.13 | 1.13 | 1.13 | 1.13 | 1.30 | 1.85 | 2.76 | 2.95 | 1.67 | 1.04 | 1.70 | 1.76 |
| Lu | 0.03 | 0.03 | 0.05 | 0.05 | 0.02 | 0.01 | 0.03 | 0.17 | 0.17 | 0.17 | 0.17 | 0.19 | 0.28 | 0.44 | 0.46 | 0.25 | 0.15 | 0.26 | 0.26 |
| Hf | 0.66 | 0.62 | 0.31 | 0.29 | 0.12 | 0.10 | 0.25 | 2.61 | 2.57 | 2.61 | 2.57 | 1.93 | 3.15 | 6.21 | 6.16 | 2.49 | 1.44 | 2.50 | 2.26 |
| Ta | 0.11 | 0.11 | 0.08 | 0.06 | 0.03 | 0.04 | 0.13 | 0.52 | 0.51 | 0.52 | 0.51 | 0.21 | 0.32 | 0.59 | 0.72 | 0.27 | 0.14 | 0.28 | 0.26 |
| W | 0.62 | 0.85 | 0.67 | 1.33 | 0.50 | 0.49 | 0.15 | 0.53 | 0.57 | 0.53 | 0.57 | 0.42 | 0.52 | 0.66 | 0.86 | 0.59 | 0.35 | 0.58 | 1.48 |
| Pb | 0.18 | 0.26 | 1.42 | 1.59 | 0.08 | 0.21 | 43.71 | 14.57 | 14.06 | 14.57 | 14.06 | 3.54 | 2.30 | 8.92 | 7.98 | 5.43 | 5.75 | 5.19 | 5.44 |
| Bi | 0.00 | 0.00 | 0.31 | 0.31 | 0.01 | 0.00 | 0.25 | 0.31 | 0.31 | 0.31 | 0.31 | 0.03 | 0.07 | 0.16 | 0.20 | 0.08 | 0.05 | 0.08 | 0.03 |
| Th | 1.54 | 1.55 | 0.69 | 0.72 | 0.20 | 0.19 | 0.00 | 2.29 | 2.64 | 2.29 | 2.64 | 1.14 | 2.35 | 7.99 | 10.24 | 2.84 | 0.56 | 2.87 | 2.88 |
| U | 0.81 | 0.80 | 0.57 | 0.59 | 0.28 | 0.28 | 0.20 | 0.51 | 0.55 | 0.51 | 0.55 | 0.34 | 0.59 | 1.23 | 1.58 | 0.33 | 0.14 | 0.33 | 0.45 |

Figure 1

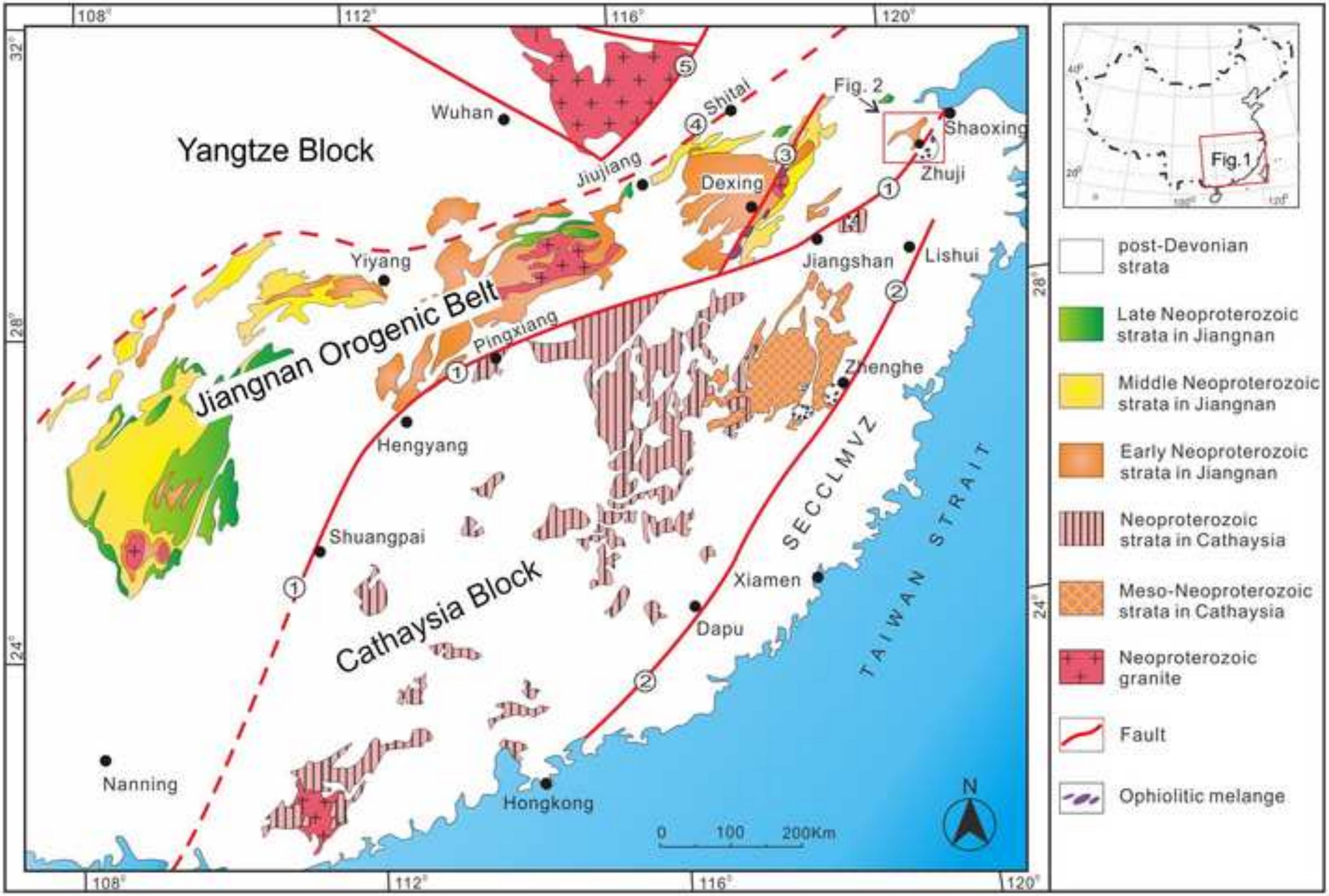

Yangtze Block
Jiangnan Orogenic Belt
Cathaysia Block
Wuhan
Shitai
Jiujiang
Dexing
Fig. 2
Shaoxing
Zhuji
Jiangshan
Lishui
Yiyang
Pingxiang
Zhenghe
Hengyang
Shuangpai
Xiamen
Dapu
Nanning
Hongkong
SECCLMVZ
TAIWAN STRAIT
0 100 200Km
N
Fig. 1
108°
112°
116°
120°
32°
28°
24°
post-Devonian strata
Late Neoproterozoic strata in Jiangnan
Middle Neoproterozoic strata in Jiangnan
Early Neoproterozoic strata in Jiangnan
Neoproterozoic strata in Cathaysia
Meso-Neoproterozoic strata in Cathaysia
Neoproterozoic granite
Fault
Ophiolitic melange

Figure 2

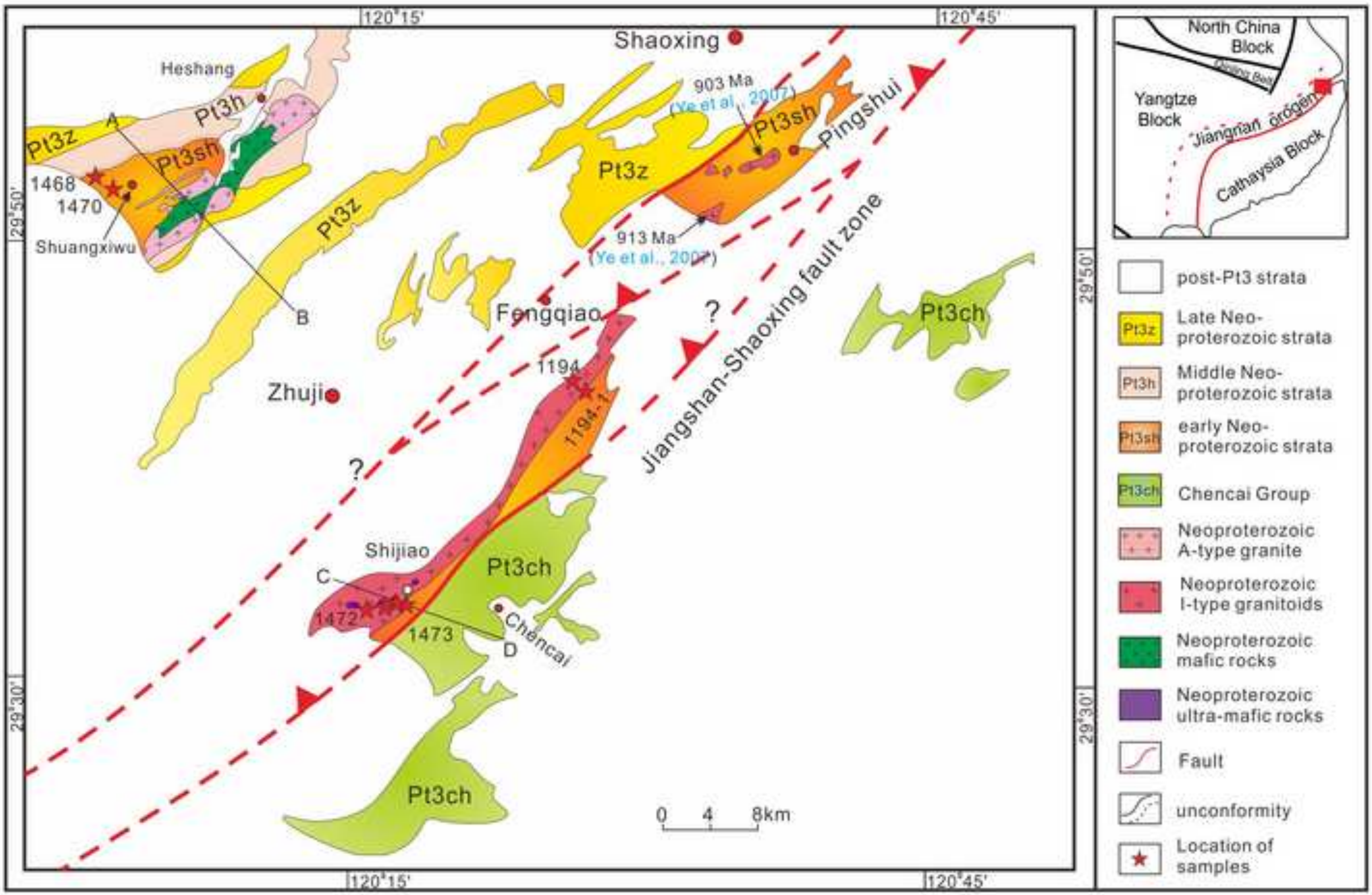
120°15'
120°45'
29°50'
29°30'
Shaoxing
Heshang
Pt3h
Pt3z
Pt3sh
A
B
1468
1470
Shuangxiwu
903 Ma
(Ye et al., 2007)
913 Ma
(Ye et al., 2007)
Pingshui
Fengqiao
Zhuji
1194
1194-1
?
Jiangshan-Shaoxing fault zone
Pt3ch
Shijiao
C
D
1472
1473
Chencai
0 4 8km
North China Block
Yangtze Block
Jiangnan orogen
Cathaysia Block
post-Pt3 strata
Late Neo-proterozoic strata
Middle Neo-proterozoic strata
early Neo-proterozoic strata
Chencai Group
Neoproterozoic A-type granite
Neoproterozoic I-type granitoids
Neoproterozoic mafic rocks
Neoproterozoic ultra-mafic rocks
Fault
unconformity
Location of samples

Figure 3

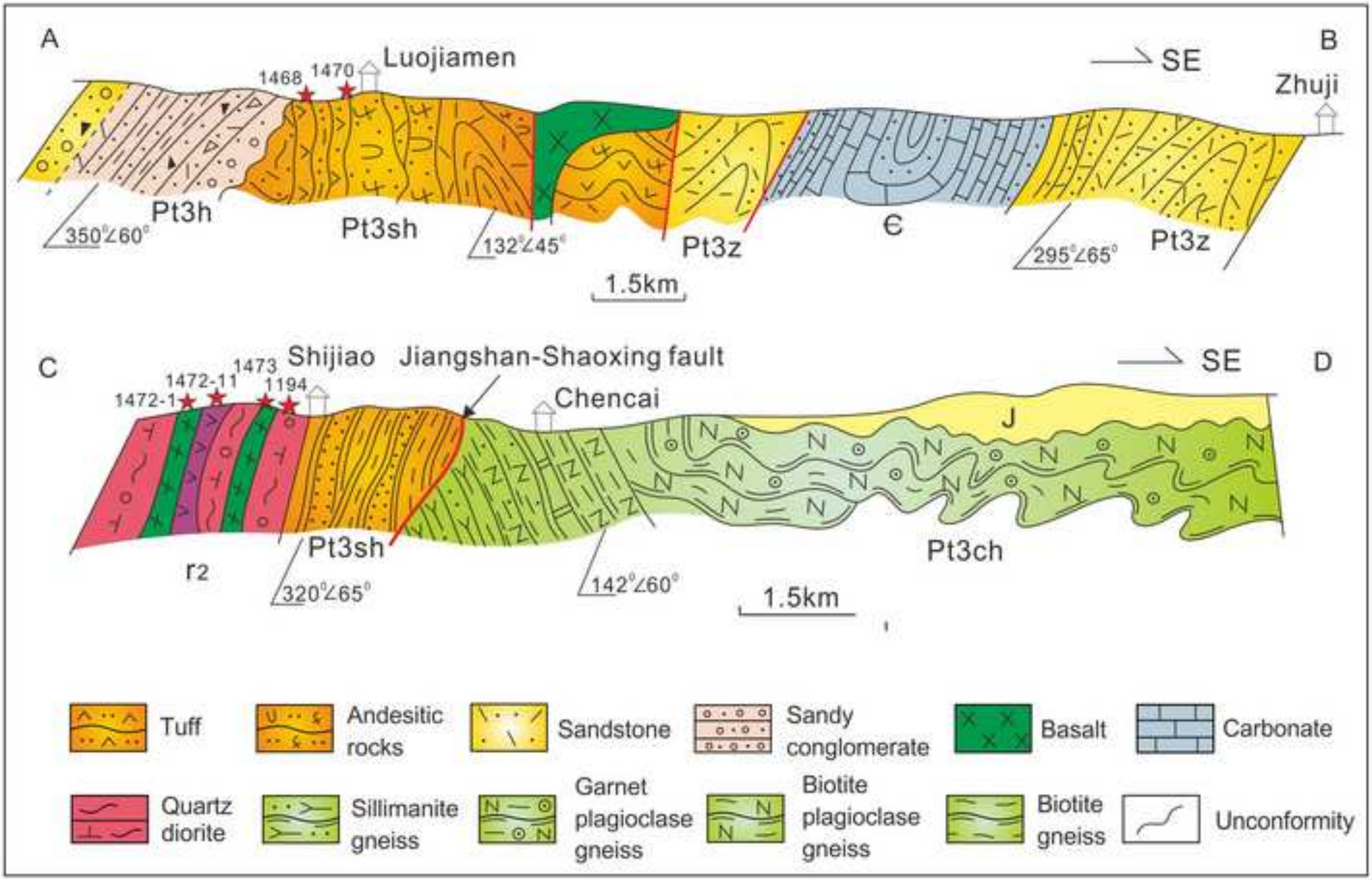
A
B
SE
Luojiamen
Zhuji
1468
1470
Pt3h
Pt3sh
Pt3z
Є
Pt3z
350°∠60°
132°∠45°
295°∠65°
1.5km
C
D
SE
Shijiao
Jiangshan-Shaoxing fault
Chencai
1472-1
1472-11
1473
1194
J
Pt3sh
Pt3ch
r2
320°∠65°
142°∠60°
1.5km
Tuff
Andesitic rocks
Sandstone
Sandy conglomerate
Basalt
Carbonate
Quartz diorite
Sillimanite gneiss
Garnet plagioclase gneiss
Biotite plagioclase gneiss
Biotite gneiss
Unconformity


A
B
C
D
Gabbro
Dunite
E
F

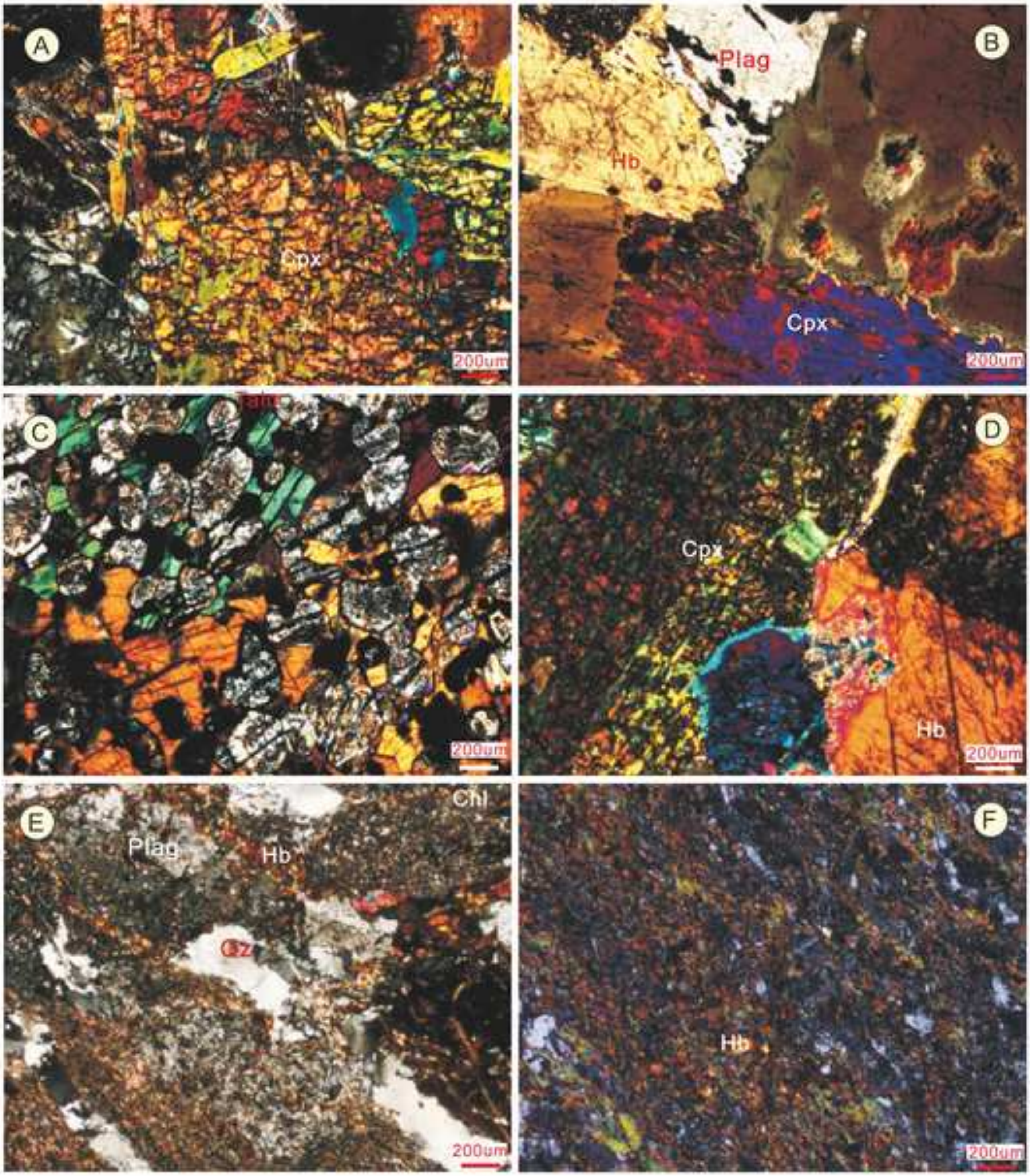
A
Cpx
200um
B
Plag
Hb
Cpx
200um
C
200um
D
Cpx
Hb
200um
E
Chl
Plag
Hb
Qz
200um
F
Hb
200um

Figure 6

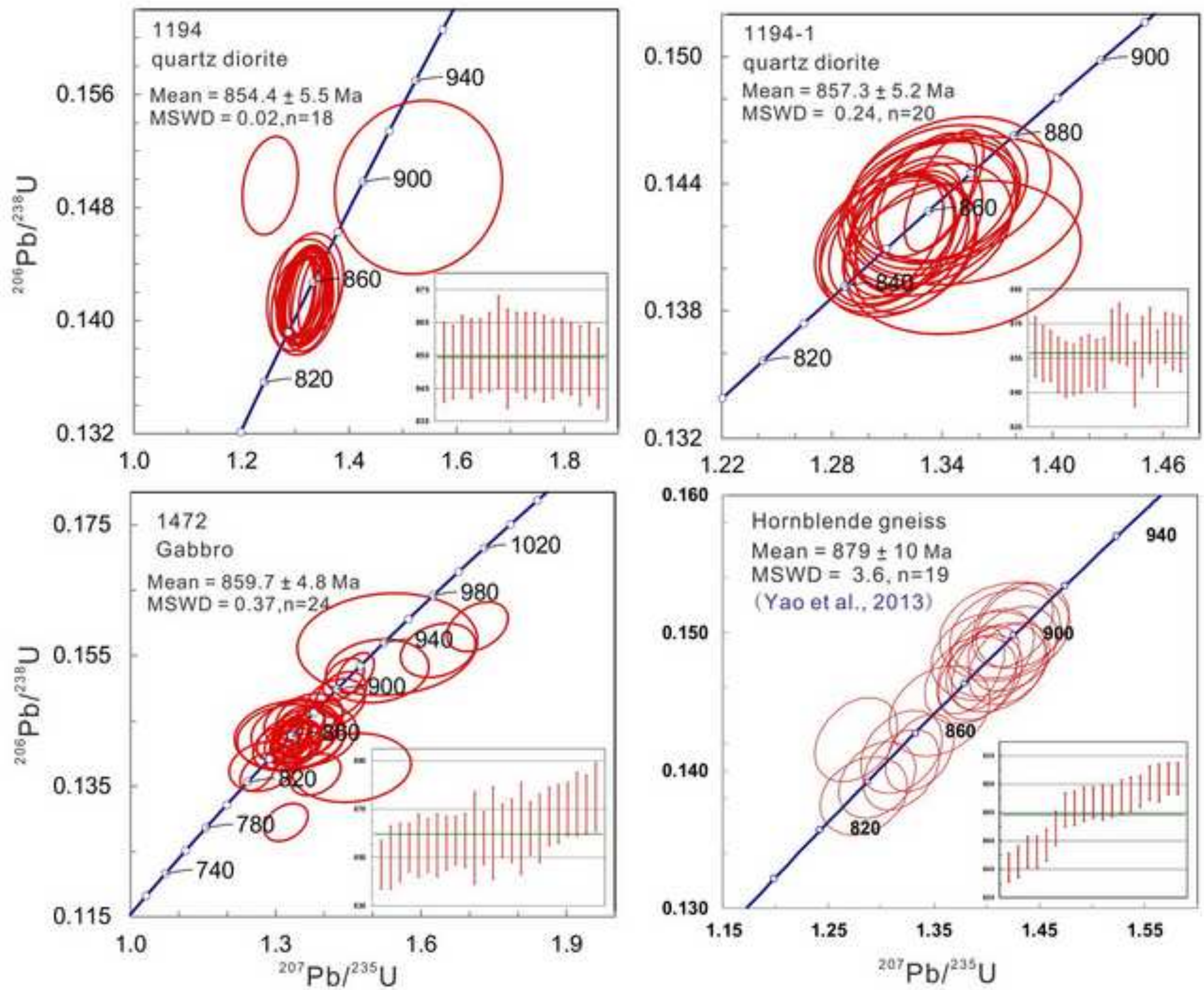

1194
quartz diorite
Mean = 854.4 ± 5.5 Ma
MSWD = 0.02,n=18
1194-1
quartz diorite
Mean = 857.3 ± 5.2 Ma
MSWD = 0.24, n=20
1472
Gabbro
Mean = 859.7 ± 4.8 Ma
MSWD = 0.37,n=24
Hornblende gneiss
Mean = 879 ± 10 Ma
MSWD = 3.6, n=19
(Yao et al., 2013)
206Pb/238U
207Pb/235U

Figure 7

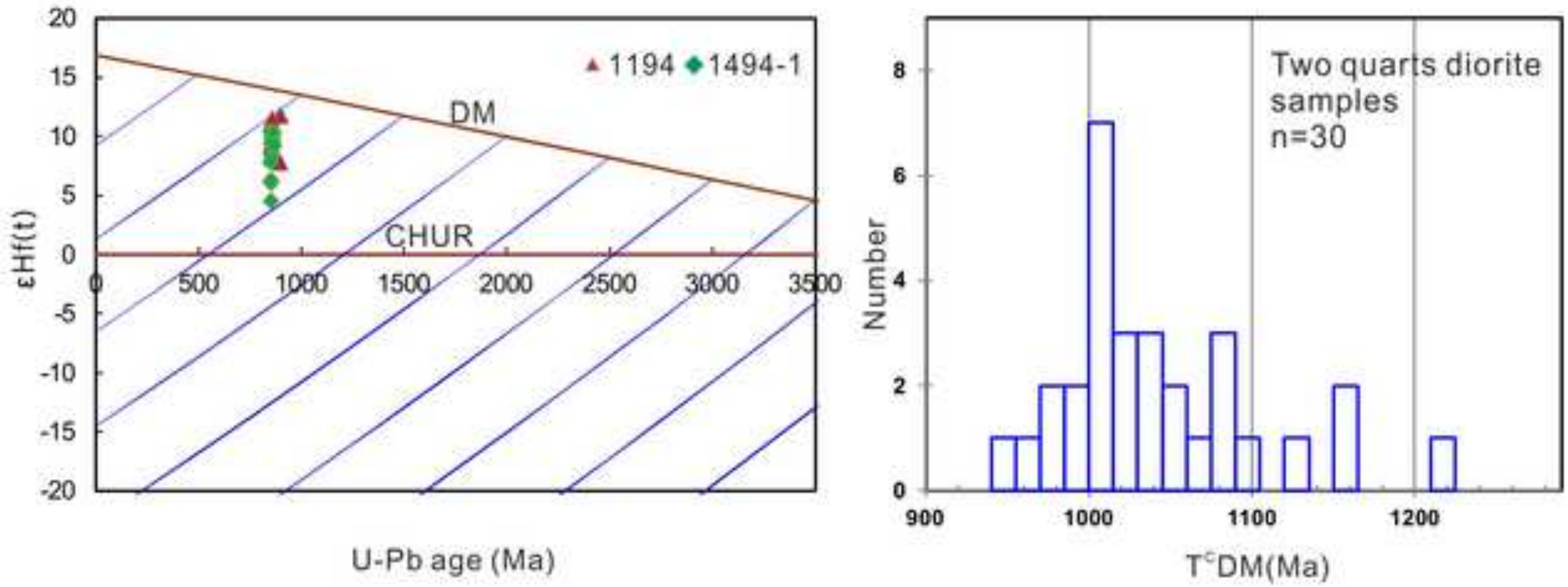
1194
1494-1
DM
CHUR
εHf(t)
U-Pb age (Ma)
Two quarts diorite samples
n=30
Number
T^cDM(Ma)

Figure 8

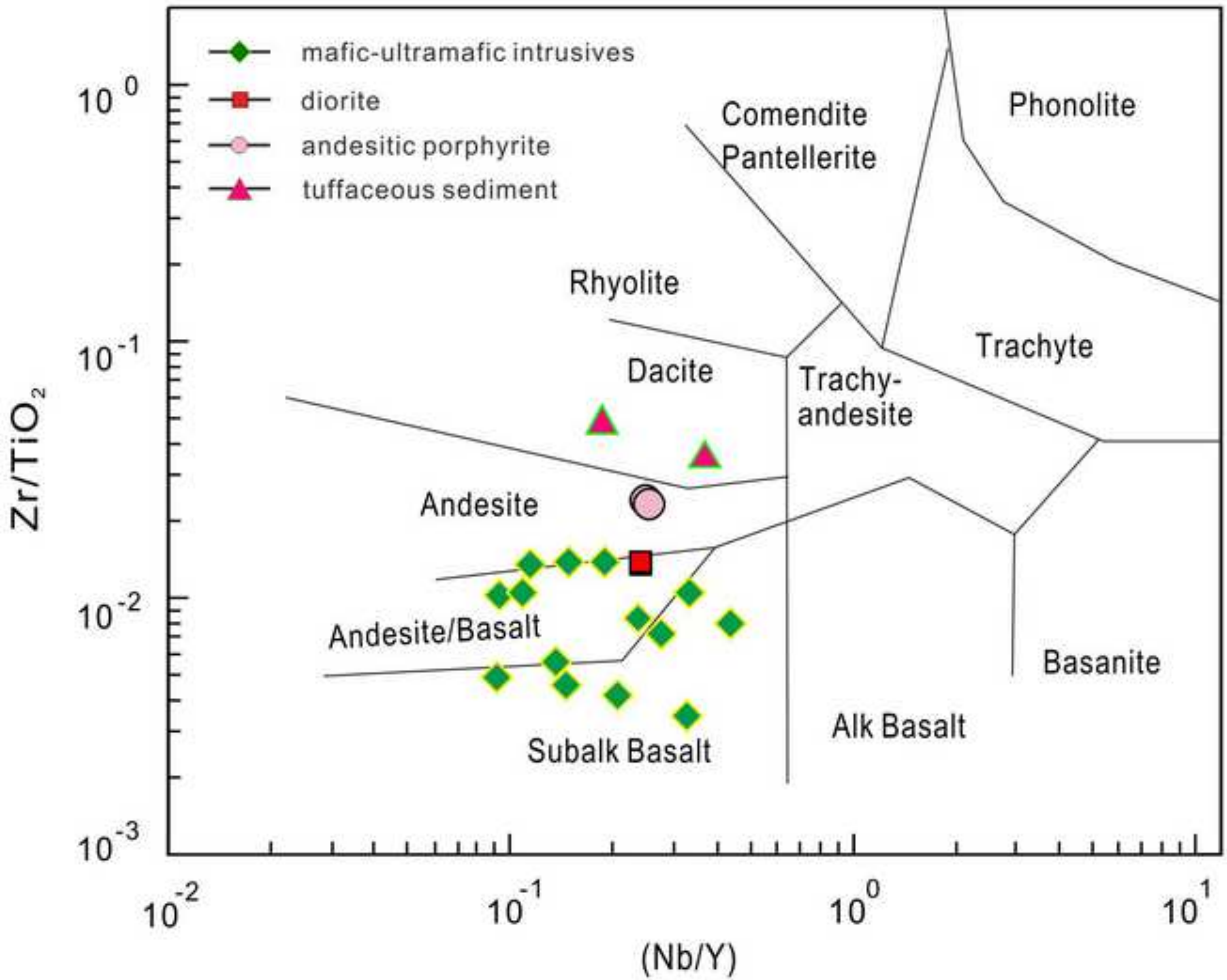
mafic-ultramafic intrusives
diorite
andesitic porphyrite
tuffaceous sediment
Comendite
Pantellerite
Phonolite
Rhyolite
Dacite
Trachy-
andesite
Trachyte
Andesite
Andesite/Basalt
Basanite
Alk Basalt
Subalk Basalt
Zr/TiO2
(Nb/Y)
$10^{0}$
$10^{-1}$
$10^{-2}$
$10^{-3}$
$10^{-2}$
$10^{-1}$
$10^{0}$
$10^{1}$

**Figure 9**

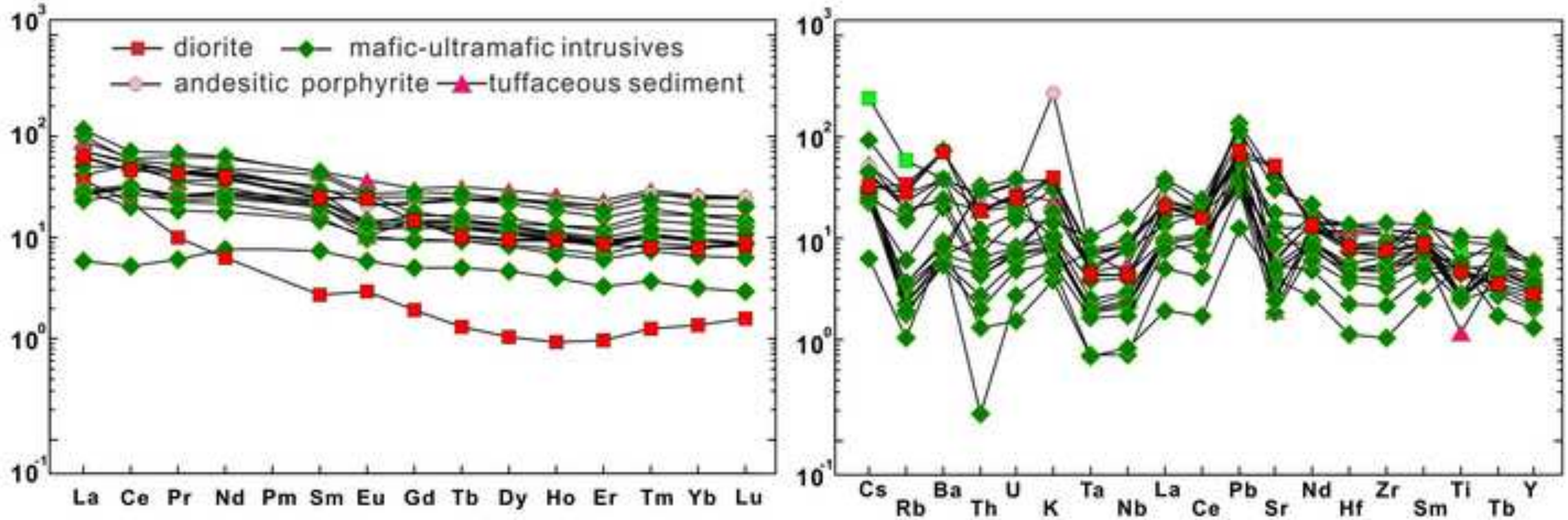

diorite
mafic-ultramafic intrusives
andesitic porphyrite
tuffaceous sediment
$10^3$
$10^2$
$10^1$
$10^0$
$10^{-1}$
La Ce Pr Nd Pm Sm Eu Gd Tb Dy Ho Er Tm Yb Lu
Cs Rb Ba Th U K Ta Nb La Ce Pb Sr Nd Hf Zr Sm Ti Tb Y

**Figure 10**

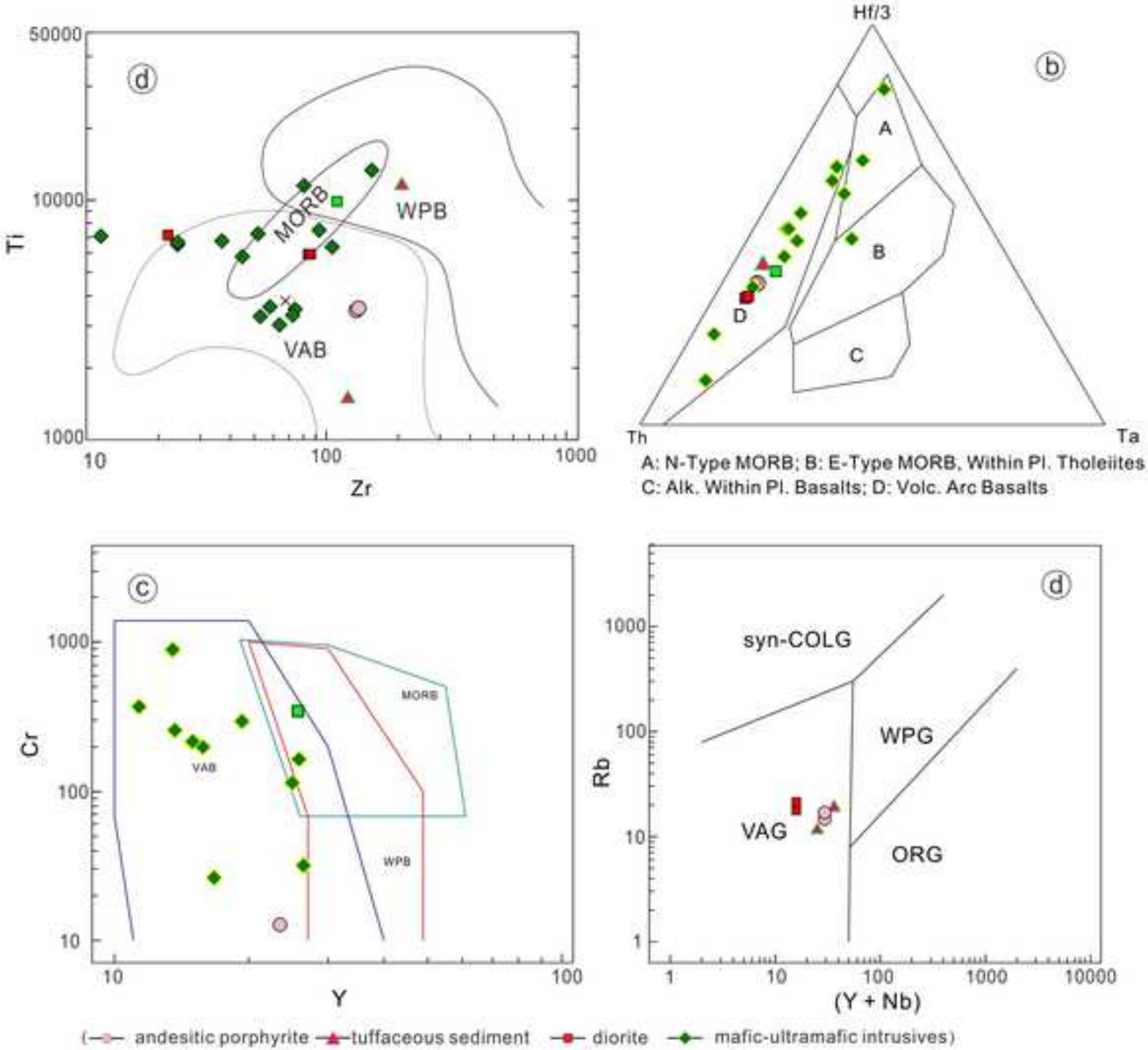
d
50000
10000
1000
Ti
MORB
WPB
VAB
10
100
1000
Zr
Hf/3
b
A
B
C
D
Th
Ta
A: N-Type MORB; B: E-Type MORB, Within Pl. Tholeiites
C: Alk. Within Pl. Basalts; D: Volc. Arc Basalts
c
1000
100
10
Cr
MORB
VAB
WPB
Y
d
syn-COLG
WPG
VAG
ORG
Rb
1
10000
(Y + Nb)
andesitic porphyrite
tuffaceous sediment
diorite
mafic-ultramafic intrusives

**Figure 11**

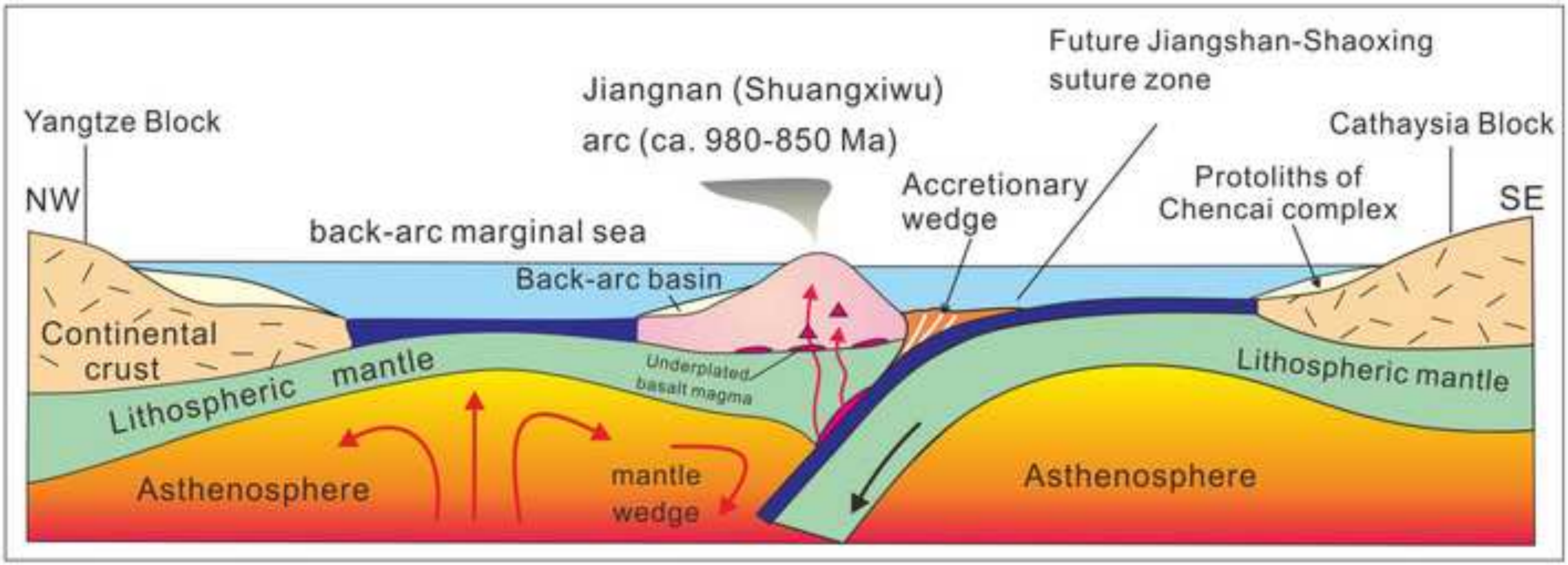

Future Jiangshan-Shaoxing
suture zone
Jiangnan (Shuangxiwu)
arc (ca. 980-850 Ma)
Yangtze Block
Cathaysia Block
NW
SE
Accretionary
wedge
Protoliths of
Chencai complex
back-arc marginal sea
Back-arc basin
Continental
crust
Lithospheric mantle
Underplated
basalt magma
Lithospheric mantle
Asthenosphere
mantle
wedge
Asthenosphere

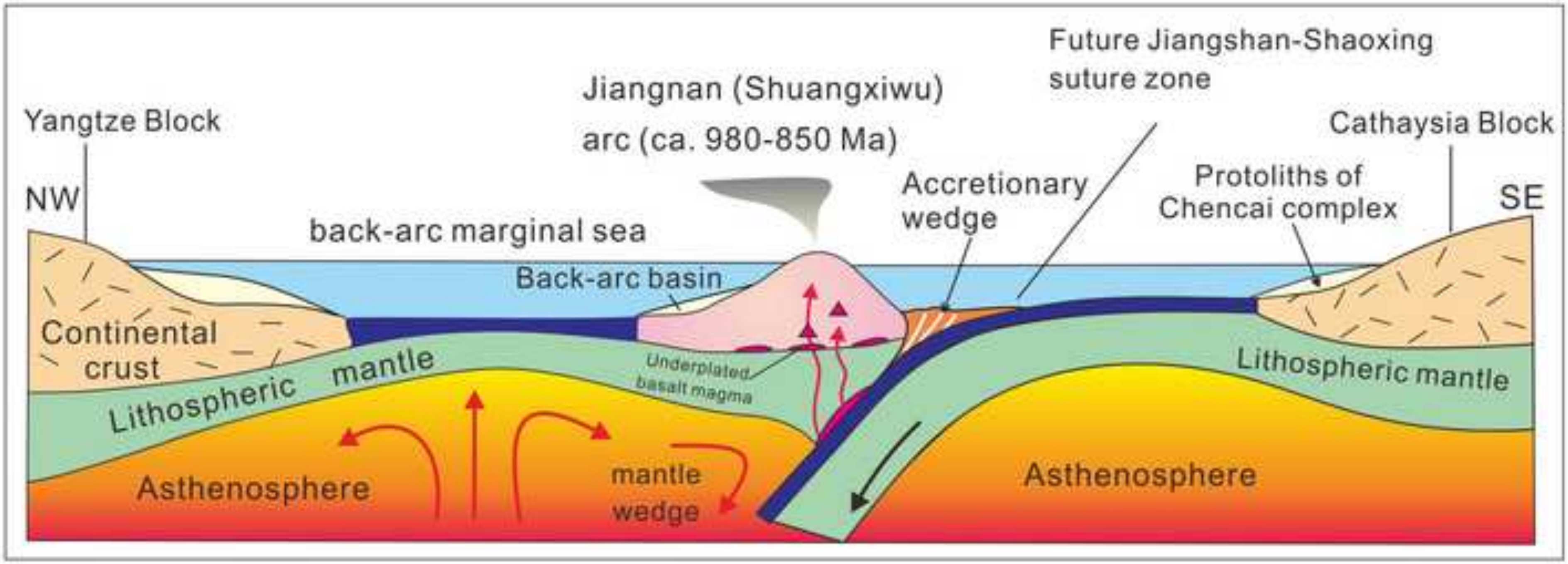

Future Jiangshan-Shaoxing
suture zone
Jiangnan (Shuangxiwu)
arc (ca. 980-850 Ma)
Yangtze Block
Cathaysia Block
NW
SE
Accretionary
wedge
Protoliths of
Chencai complex
back-arc marginal sea
Back-arc basin
Continental
crust
Lithospheric mantle
Underplated
basalt magma
Lithospheric mantle
Asthenosphere
mantle
wedge
Asthenosphere